NASA Technical Memorandum 78558

Inhomogeneous Models of the Venus Clouds Containing Sulfur

Sheldon M. Smith, James B. Pollack,
Lawrence P. Giver, Jeffrey N. Cuzzi,
and Morris Podolak

April 1979

National Aeronautics and
Space Administration

NASA Technical Memorandum 78558

Inhomogeneous Models of the Venus Clouds Containing Sulfur

Sheldon M. Smith
James B. Pollack
Lawrence P. Giver
Jeffrey N. Cuzzi
Morris Podolak, Ames Research Center, Moffett Field, California

National Aeronautics and
Space Administration

Ames Research Center
Moffett Field, California 94035

INHOMOGENEOUS MODELS OF THE VENUS CLOUDS CONTAINING SULFUR

Sheldon M. Smith, James B. Pollack, Lawrence P. Giver, Jeffrey N. Cuzzi, and Morris Podolak*

Ames Research Center

ABSTRACT

On the basis of A. T. Young's suggestion that elemental sulfur is responsible for the yellow color of Venus, we compare calculations at 3.4 μm of the reflectivity phase function of two sulfur containing inhomogeneous cloud models with that of the homogeneous model of Hansen and Hovenier. The inhomogeneous drop model has a spherical core of solid sulfur within each sulfuric acid drop, while the inhomogeneous cloud model has a bimodal size distribution with irregular sulfur particles comprising the second size mode near 13 μm. The calculations were made at 3.4 μm because the ability to detect small contributions from non-absorbing species to the sunlight scattered by the Venus clouds is greatly enhanced (~40 times) in the infrared absorption band of sulfuric acid. Assuming reflectivity observations with 25% or less total error, comparison of the model calculations leads to a minimum detectable mass of sulfur equal to 7% of the mass of sulfuric acid for the inhomogeneous drop model. For the inhomogeneous cloud model the comparison leads to a minimum detectable mass of sulfur between 17% and 38% of the mass of the acid drops, depending upon the actual size of the large particles. That amount of sulfur is equivalent to detecting about one large sulfur particle per 10^4 sulfuric acid drops. We conclude that moderately accurate 3.4 μm reflectivity observations are capable of detecting quite small amounts of elemental sulfur at the top of the Venus clouds.

*Tel-Aviv University, Tel-Aviv, Israel

INTRODUCTION

It is generally well accepted that sulfuric acid is the principal constituent of the Venus clouds, and that the planet's yellow color is caused by absorption of the blue end of the reflected solar spectrum. It is also known that sulfuric acid is transparent in the blue and visible, and is thus incapable of producing the yellow color of the planet. Such reasoning suggests that an additional cloud constituent be considered.

There are three ways in which an additional blue absorber could be added to the Venus cloud aerosol. The first has the additional constituent completely dissolved in the liquid sulfuric acid cloud drops, and the second places the constituent as a solid core inside each liquid drop. In the third way, particles (or drops) of the blue absorber are mixed inhomogeneously among the acid drops of the clouds. A fourth way, which we shall not treat here, adds the blue absorber to the cloud as an unknown gas.

Recently, A. T. Young (ref. 1) amplified an earlier suggestion by Hapke (ref. 2) that elemental sulfur is the additional absorber because it has a temperature sensitive blue absorption edge capable of explaining the visual color of Venus. If sulfur is the new constituent, it is not added to the clouds in the first way described above because sulfur does not dissolve in sulfuric acid (personal communication, O. B. Toon, Ames Research Center, 1978). However the other two ways, the inhomogeneous drop and the inhomogeneous cloud, are distinct possibilities. Young (ref. 1) has already proposed an inhomogeneous cloud model in which 1% of the number density of acid drops are large (~13 μm) sulfur particles buried in a cloud just below that from which most of the sulfuric acid scattering is observed, that is, at $\tau > 4$ for visual wavelengths. Thus, these sulfur particles are well hidden in the visual and they would affect the spectrum primarily through their strong ultraviolet absorption.

For the following reasons we suggest utilizing the infrared reflectivity of Venus to investigate such inhomogeneous models. First, scattering at intermediate backscatter angles by the cloud drops themselves is greatly reduced in the infrared absorption bands of H_2SO_4. However, backscattering by nonabsorbing species, such as sulfur, is not so reduced and thus can be more easily detected. Second, the absorption is so strong that single scattering is the predominant radiative transfer process within the clouds. Third, the quite large size and irregular shape of the proposed sulfur particles will also assist their detection at 3 μm wavelengths.

To evaluate our suggestion, we have calculated the reflectivity of Venus at 3.4 μm for two inhomogeneous models using a Mie scattering doubling routine which we modified to contain either an inhomogeneous drop with a sulfur core, or a bimodal particle-size distribution with large, nonspherical sulfur particles in the second peak. We have also calculated the homogeneous drop-homogeneous

cloud model of Hansen and Hovenier (ref. 3) for comparison. These models and representative calculations are presented in considerable detail in the next section in order to describe them and a new type of reflectivity function under a variety of conditions. In the third section we discuss the models; show the dependence of their backscattering on the core volume or particle area; evaluate the amount of sulfur that absolute observations at 3.4 μm could detect by comparison with them; and calculate the height to which the observations penetrate.

MODELS AND DEMONSTRATION CALCULATIONS

The Reflectivity Function

We have chosen to define a reflectivity function, $\tilde{R}(\lambda,\phi)$, for the Venus cloud top that is an average of the directional reflectivity over the illuminated fraction of the planet's disk. This is a convenient choice because when absorption is strong, the shape of the phase angle dependence of the reflectivity function is very similar to that of the single scattering phase function and so facilitates comparison of telescopic observations with cloud drop models. This definition has already been used by one of us (Pollack, ref. 4) to describe reflection spectra of Venus between 1.2 and 4.0 μm.

The reflectivity of a cloud or atmosphere is fundamentally related to the wavelength of the incident light, λ, and to the scattering angle, θ. Hence, the reflectivity function is an intrinsic function of wavelength and angle. We write it as $\tilde{R}(\lambda,\phi)$ because the planetary phase angle ϕ is the supplement of θ and is easily obtained from the Ephemeris. Unfortunately, the observed infrared flux from Venus depends both implicitly and explicitly on several other variables that mask the λ, ϕ dependence of the reflectivity. To elucidate that dependence, we write the monochromatic flux received at Earth, $F(\lambda,\phi,T,r_{\varphi-\oplus})$, as the sum of two Lambertian surface brightnesses multiplied by the appropriate solid angles. The first term represents reflected light and the second term thermal emission

$$F(\lambda,\phi,T,r_{\varphi-\oplus}) = \frac{\tilde{R}(\lambda,\phi)F_{\odot-\varphi}(\lambda,r_{\odot-\varphi})}{\pi}\left(\frac{\frac{1+\cos\phi}{2}\pi R_{\varphi}^{2}}{r_{\varphi-\oplus}^{2}}\right) + \frac{\varepsilon(\lambda)W(\lambda,T)}{\pi}\left(\frac{\pi R_{\varphi}^{2}}{r_{\varphi-\oplus}^{2}}\right) \quad (1)$$

In equation (1), R_{φ} is the semidiameter of Venus, $r_{\varphi-\oplus}$ is the Venus-Earth distance, and $r_{\odot-\varphi}$ is the Sun-Venus distance. The thermal spectral emittance is represented by a Planck function, $\varepsilon(\lambda)W(\lambda,T)$, in which a uniform effective temperature T is a good approximation for the entire disk of Venus on both the illuminated and dark sides. Equation (1) treats the spectral reflectance $\tilde{R}(\lambda,\phi)F_{\odot-\varphi}(\lambda,r_{\odot-\varphi})$ in the same manner as the thermal spectral emittance after multiplication of the solar spectral irradiance, $F_{\odot-\varphi}(\lambda,r_{\odot-\varphi})$, by $\tilde{R}(\lambda,\phi)$ has converted the irradiance to a reflectance. Dividing both fluxes by π sr converts them into Lambertian radiances for normal incidence. Thus, the reflectivity function $\tilde{R}(\lambda,\phi)$ is an average reflectivity over the illuminated portion of the Venus disk.

The phase-angle dependence of the atmosphere's reflectivity is now contained solely in $\tilde{R}(\lambda,\phi)$, although ϕ also appears as $(1 + \cos \phi)/2$ in the solid-angle factor. That factor describes only the fraction of the area of the disk that is illuminated and has nothing to do with the optical properties of Venus' atmosphere. This point should be emphasized. Most phase functions of Venus are plots of reflected flux versus phase angle; therefore, they are heavily weighted by $(1 + \cos \phi)/2$. We have separated out that factor, so the reflectivity function just defined pertains only to an average segment of the illuminated atmosphere and is independent of illuminated area.

For ease in comparing $\tilde{R}(\lambda,\phi)$ to related quantities defined by others, equation (1) may be rewritten as

$$\tilde{R}(\lambda,\phi) = \frac{F(\lambda,\phi,T,r_{\varphi-\oplus})S^{-2}_{(r_{\varphi-\oplus})} - \varepsilon(\lambda)W(\lambda,T)}{\frac{1 + \cos \phi}{2} F_{\odot-\varphi}(\lambda,r_{\odot-\varphi})} \tag{2}$$

where $S_{(r_{\varphi-\oplus})} = R_{\varphi}/r_{\varphi-\oplus}$. The thermal term is insignificant at $\lambda < 3$ μm. In this article we will be concerned with observations at $\lambda = 3.4$ μm, where the reflected flux still dominates the thermal contribution. However, near inferior conjunction it may become necessary to correct observational data for the thermal component when determining $\tilde{R}(\lambda,\phi)$.

We now compare $\tilde{R}(\lambda,\phi)$ to the geometric albedo, $p(\lambda,\phi)$. In reference 5 the albedo of Venus at unit distance from both the Sun and Earth is calculated as

$$\log_{10} p(\lambda,\phi,1) = 0.4[m_{\odot} - m(1,\phi)] - 2 \log_{10}(\sin \sigma_1') \tag{3}$$

where $m_{\odot}$ is the apparent magnitude of the Sun at wavelength λ; $m(1,\phi)$ is the apparent magnitude of the planet at wavelength λ if the planet were at a distance of 1 AU (astronomical unit) from both the Sun and the Earth; and σ_1' is the radius of the circle having the same projected area on the sky as the planet's disk at 1 AU from Earth. Converting magnitude to flux and σ_1' to solid angle, the geometric albedo is

$$p(\lambda,\phi,1) = \frac{F(\lambda,\phi,1 \text{ AU})}{S_{\varphi}^{2}(1 \text{ AU}) F_{\odot}(\lambda,1 \text{ AU}) \left(\frac{1 \text{ AU}}{r_{\odot-\varphi}}\right)^2} \tag{4}$$

where $F_{\odot}(\lambda,1 \text{ AU})$ is the solar spectral irradiation at Earth and $F(\lambda,\phi,1 \text{ AU})$ is the flux that would be received from Venus if $r_{\varphi-\oplus} = 1$ AU. But

$$F_{\odot-\varphi}(\lambda,r_{\odot-\varphi}) = F_{\odot}(\lambda,1 \text{ AU}) \left(\frac{1 \text{ AU}}{r_{\odot-\varphi}}\right)^2 \tag{5}$$

and

$$\frac{F(\lambda,\phi,r_{\varphi-\oplus})}{S_{\varphi}^{2}(r_{\varphi-\oplus})} = \frac{F(\lambda,\phi,1\ AU)}{S_{\varphi}^{2}(1\ AU)} \tag{6}$$

so that

$$p(\lambda,\phi) = \frac{F(\lambda,\phi,r_{\varphi-\oplus})}{S_{\varphi}^{2}(r_{\varphi-\oplus})F_{\odot-\varphi}(\lambda,r_{\odot-\varphi})} \tag{7}$$

This definition is valid at wavelengths where thermal emission is negligible. Where that is the case we can omit the thermal term in equation (2), and then

$$\tilde{R}(\lambda,\phi) = \frac{p(\lambda,\phi)}{\left(\frac{1+\cos\phi}{2}\right)} \tag{8}$$

Thus, our reflectivity function is just the geometric albedo divided by the illuminated fraction of the planetary disk.

The Bond (or spherical) albedo of a planet is the probability that a photon will be scattered by the planet. It is defined as the ratio of the flux reflected at all angles to the incident solar flux at $\phi = 0$, and expressed in reference 5 as

$$A(\lambda) = p(\lambda,0)q(\lambda) \tag{9}$$

where $q(\lambda)$ is the phase integral

$$q(\lambda) = 2\int_{0}^{\pi} \Phi(\lambda,\phi)\sin(\phi)d\phi \tag{10}$$

In equation (10), $\Phi(\lambda,\phi)$ is the flux density seen by the observer normalized to unity at full phase; reference 5 expresses this in magnitudes as

$$\log_{10}\Phi(\lambda,\phi) = 0.4[m(\lambda,1\ AU,0) - m(\lambda,1\ AU,\phi)] \tag{11}$$

In flux units this is

$$\Phi(\lambda,\phi) = \frac{F(\lambda,\phi,1\ AU)}{F(\lambda,0,1\ AU)} \tag{12}$$

which, from equations (4) and (8) is simply

$$\Phi(\lambda,\phi) = \frac{p(\lambda,\phi)}{p(\lambda,0)} = \frac{\tilde{R}(\lambda,\phi)\left(\frac{1+\cos\phi}{2}\right)}{\tilde{R}(\lambda,0)} \tag{13}$$

Thus, equation (9) for the Bond albedo can be written in terms of the reflectivity function as

$$A(\lambda) = 2\tilde{R}(\lambda,0)\int_0^{\pi} \frac{\tilde{R}(\lambda,\phi)\,\frac{1+\cos\phi}{2}}{\tilde{R}(\lambda,0)} \sin\phi\, d\phi$$

or

$$A(\lambda) = \int_0^{\pi} \tilde{R}(\lambda,\phi)(1+\cos\phi)\sin\phi\, d\phi \tag{14}$$

The Bond albedo of Venus is difficult to evaluate from observation alone because at very small phase angles the planet passes behind the Sun. Calculation of $\tilde{R}(\lambda,\phi)$ from theoretical models can then be used as ϕ approaches zero to supplement observations in the evaluation of $A(\lambda)$ through (14).

In summary, we have defined a reflectivity function that is an average directional reflectivity over the illuminated part of the Venus disk and whose shape is similar to that of the single scattering phase function for strong absorption. It is not the usually defined planetary phase function, and its shape is very different from that of the geometric albedo. It can be easily integrated to produce the Bond (or spherical) albedo.

Homogeneous Drop-Homogeneous Cloud Model

In recent years our understanding of the Venus clouds has been vastly improved through calculation of the multiple scattering of polarized light in a homogeneous model atmosphere (ref. 3). To provide a framework in which to place the modifications that produce the inhomogeneous models which follow, we first outline the homogeneous calculation as described by Hansen and Travis (ref. 6). This calculation is usually divided into two parts: (1) single scattering by independent scatterers within a small volume element, and (2) multiple scattering by homogeneous layers of the entire atmosphere. Because our inhomogeneous modifications affect primarily the single scattering part of the calculation, we will describe that part quite fully.

At the heart of the single scattering problem lie the Mie electric and magnetic multipole coefficients, a_n and b_n. They are formed from combinations of Ricatti-Bessel functions, and are functions of only the complex index of refraction, $m = n_r - in_i$, and the size parameter, $x = 2\pi r/\lambda$, where r is the particle radius and λ is the wavelength. The scattering and absorption cross sections, as well as the single scattering phase function, can be found from these coefficients following the Mie theory (see refs. 7, 8).

Let the single scattering cross section σ_s be written as

$$\sigma_s = \pi r^2 Q_s \tag{15}$$

where Q_s is the efficiency factor for scattering. Similar expressions can be written for the absorption and extinction (scattering + absorption) cross sections. Van de Hulst (ref. 7) has shown that

$$Q_s = \frac{2}{x^2} \sum_{n=1}^{\infty} (2n + 1)(|a_n|^2 + |b_n|^2) \tag{16}$$

and

$$Q_e = \frac{2}{x^2} \sum_{n=1}^{\infty} (2n + 1)\mathcal{R}_e(a_n + b_n) \tag{17}$$

where Q_e is the efficiency factor for extinction. The efficiency factor for absorption Q_a can be obtained from $Q_e - Q_s$. Van de Hulst also writes the single-scattering phase function $P^{11}(r,\theta)$ for the unpolarized intensity as

$$P^{11}_{(r,\theta)} = \frac{\lambda^2}{2\pi\sigma_s(r)} \left[|S_1(r,\theta)|^2 + |S_2(r,\theta)|^2\right] \tag{18}$$

where

$$S_1(r,\theta) = \sum_{n=1}^{\infty} \frac{2n + 1}{n(n + 1)} [a_n\pi_n(\cos\theta) + b_n\tau_n(\cos\theta)] \tag{19}$$

$$S_2(r,\theta) = \sum_{n=1}^{\infty} \frac{2n + 1}{n(n + 1)} [b_n\pi_n(\cos\theta) + a_n\tau_n(\cos\theta)] \tag{20}$$

The superscript 11 indicates that $P^{11}(r,\theta)$ is the first element of the 4×4 phase matrix which completely describes the angular distribution and polarization of the scattered light. Here π_n and τ_n are functions of θ, the scattering angle, and can be written in terms of the Legendre polynomials. Note that θ is the supplement of the planetary phase angle ϕ used in the preceding section.

In practice, we used a computer program due to Dave,[1] which computes the Legendre polynomials and Ricatti-Bessel functions from recurrence relations. The coefficients π_n and τ_n are calculated for specified scattering angles using straightforward upward recurrence relations based on the well-known properties of the Legendre polynomials and their derivatives.

[1]Dave, J. V.: Subroutines for Computing the Parameters of the Electromagnetic Radiation Scattered by a Sphere. IBM Report 320-3237, 1968.

For specific particle radii, the Mie coefficients are calculated from:

$$a_n(z) = \frac{\left[\frac{A_n(z)}{m} + \frac{n}{x}\right] \mathrm{Re}\zeta_n(x) - \mathrm{Re}\zeta_{n-1}(x)}{\left[\frac{A_n(z)}{m} + \frac{n}{x}\right] \zeta_n(x) - \zeta_{n-1}(x)} \tag{21}$$

$$b_n(z) = \frac{\left[mA_n(z) + \frac{n}{x}\right] \mathrm{Re}\zeta_n(x) - \mathrm{Re}\zeta_{n-1}(x)}{\left[mA_n(z) + \frac{n}{x}\right] \zeta_n(x) - \zeta_{n-1}(x)} \tag{22}$$

where $A_n(z) = \psi_n'(z)/\psi_n(z)$, $z = mx$ is the complex size parameter, and $\psi_n(z)$, $\zeta_n(x)$ are Ricatti-Bessel functions. Here A_n, the logarithmic derivative of $\psi_n(z)$, has been used to avoid a computer overflow problem. Unfortunately, calculation of that derivative by means of an upward recurrence relation has been found by Kattawer and Plass (ref. 9) to involve a numerical instability (growing errors) for large values of n/z. They suggested a separate downward recurrence calculation of the derivative, which we use, to avoid the instability.

The single scattering problem is completed by integrating the phase function and efficiency factors calculated for specific particle radii over the distribution of particle sizes expected in each volume element. Thus

$$P_{(\theta)}^{11} = \frac{\lambda^2}{2\pi k_s} \int_{r_{min}}^{r_{max}} [|S_1(r,\theta)|^2 + |S_2(r,\theta)|^2] n(r) dr \tag{23}$$

and

$$k_e^s = \int_{r_{min}}^{r_{max}} \pi r^2 Q_e^s(r) n(r) dr = \int_{r_{min}}^{r_{max}} \sigma_e^s(r) n(r) dr \tag{24}$$

where $n(r)dr$ is the number density of particles with radii between r and $r + dr$, and k_s and k_e are the size-integrated scattering and extinction coefficients. In the homogeneous model, we use the "standard" size distribution employed by Hansen (ref. 10),

$$n(r) = N \frac{r^{(1-3b)/b} e^{-r/ab}}{(ab)^{(1-2b)/b} \Gamma[(1 - 2b)/b]} \tag{25}$$

where N = total number of particles per unit volume, Γ = the gamma function, and

$$a = \text{scattering effective radius} = \frac{\int_{r_{min}}^{r_{max}} r\pi r^2 n(r)dr}{\int_{r_{min}}^{r_{max}} \pi r^2 n(r)dr} \tag{25}$$

$$b = \text{scattering effective variance} = \frac{\int_{r_{min}}^{r_{max}} (r - a)^2 \pi r^2 n(r)dr}{a^2 \int_{r_{min}}^{r_{max}} \pi r^2 n(r)dr} \tag{27}$$

Because the $\int n(r)dr$ may have unusual dimensions, depending on the form of $n(r)$, it is useful to normalize the phase function as we have done in equation (23) by utilizing the size-integrated scattering coefficient. Through this normalization a dimensionless phase function is retained regardless of the exact dimensions of $\int n(r)dr$.

The multiple-scattering part of the calculation is based upon the doubling or adding method, the basis of which Hansen and Travis (ref. 6) have traced back as far as Stokes (ref. 11). The basic principle is simply that the reflection and transmission of a combination of two layers can be obtained by calculating successive reflections between layers if the reflection and transmission of each layer are known independently. The initial layers are taken to be plane-parallel and quite thin, with position inside them specified by an optical depth, $\tau = \int_h^\infty k_e n(h')dh'$, which must be summed over all species in a unit volume. If the layers are of similar composition, the results for a thick homogeneous layer can be quickly built up in a geometric (doubling) manner. If some, or all, of the layers are dissimilar the results for a thick, inhomogeneous layer are obtained more slowly by adding the contributions from each of the dissimilar layers. A recipe for the doubling routine has been given by Hansen and Travis (ref. 6), and we use a similar version developed by one of us (Pollack, ref. 12).

Calculation of the light reflected by a planet's atmosphere is completed by integrating the multiple scattering from locally plane-parallel slabs of thickness τ, such as those described above, over the illuminated portion of the spherical surface of the planet. The integration is carried out from the illuminated limb to the visible terminator by double Gaussian quadrature. The reflected flux thus calculated is divided by the product

$$\left(\frac{1 + \cos \phi}{2}\right)\left(\begin{matrix}\text{solar flux incident} \\ \text{on the planet}\end{matrix}\right)$$

to produce the absolute reflectivity function $\tilde{R}(\lambda,\phi)$ defined in the previous section.

The model calculation can be demonstrated in an interesting way by showing the strong similarity (mentioned earlier) between the shape of the single scattering phase function and that of the reflectivity function when there is strong absorption. In figure 1 we compare calculations of both at 0.55 μm for such a case (hypothetical Case No. 4 of Hansen and Travis, ref. 6). We also contrast both of them in that figure with the geometric albedo, $p(\phi)$. Here, and throughout the rest of this paper, we shall use the term backscattering to refer to light scattered at phase angles $\phi \leq 70°$, and the term forward scattering to refer to light scattered at phase angles $\phi \geq 110°$. The similar shape of the two curves is quite reasonable for the situation where absorption limits the interaction of light with the clouds to only one or two scatterings. Both functions have a characteristically steep slope because absorption within the particle strongly attenuates backscattered light while forward scattered light, due principally to diffraction, is not so attenuated. In spite of the absorption, a trace of a primary rainbow is indicated by the small peak at $\phi = 18°$. The different shape of the geometric albedo contrasts sharply with these curves indicating that $\tilde{R}(\lambda,\phi)$ is physically the more meaningful function.

The definition of the single scattering phase function, equation (23) for $P^{11}(\theta)$, indicates that only five independent parameters other than ϕ or θ need to be specified. They are λ, n_r, n_i, a, and b. The optical constants of sulfuric acid at various concentrations have been measured by Palmer and Williams (ref. 13) between 0.36 and 25 μm and by Jones (ref. 14) from 20 to 50 μm. An 85% aqueous solution is currently indicated to be the correct concentration of the Venus droplets (Pollack et al., ref. 4). The effective radius and variance of the principal droplet-size distribution, a and b, have been well determined by visible polarization measurements (Hansen and Hovenier, ref. 3). As a demonstration of the success of the multiple scattering model, we compare it in figure 2 with the observations of Irvine et al. (ref. 5) at 1.0635 μm where there is still a little H_2SO_4 absorption. The calculated reflectivity function has been multiplied by 0.899 to obtain the best fit to the observations. This factor indicates that a slight reduction of the single scattering albedo calculated from the optical constants of H_2SO_4 is required, most probably the result of our neglect of faint absorption by the very weak 1.065-μm CO_2 band (Boese et al., ref. 15). In figures 3 and 4 we demonstrate the high sensitivity of the model to variation of the real and imaginary parts of the index of refraction in the H_2SO_4 absorption band at 3.65 μm.

Both polarized visible light and unpolarized 3-4 μm light reflected from the Venus cloud tops are particularly sensitive to the high level particle size distribution because they both result from primarily single scattering processes. (The degree of polarization is reduced by multiple scattering.) Hansen and Hovenier (ref. 3) have already shown that the visible polarization is very sensitive to the value of the effective radius a and is fairly sensitive to that of the variance b. The value they determined for b (0.07) is small by terrestrial standards and could have interesting implications for the dynamics of the Venus atmosphere.

In figure 5 we demonstrate the sensitivity of the homogeneous drop-homogeneous cloud calculation at 3.65 μm to variation of the effective radius. The transition from strong forward scattering by large drops of 2.7 μm effective radius to the Rayleigh scatter by the 0.3 μm drops is quite apparent. The region of backscattered light $\phi \leq 70°$ shows high sensitivity to the value of a. In figure 6 we demonstrate the model's dependence on the effective variance. Unfortunately, it appears to be so small that Hansen and Hovenier's (ref. 3) determination of b will not be well tested in the 3-4 μm absorption band. However, their value for the effective radius clearly will be.

Finally, we contrast the 3.4 μm reflectivity function with the visual one. In figure 7 we plot them both using a = 1.05 μm, b = 0.07, m(3.4 μm) = 1.338 - 0.176i, and m(0.55 μm) = 1.44 - 0.000024i. The vastly different shape and level of the two curves is striking. In particular, the back scatter by the homogeneous model is more than 40 times smaller at 3.4 μm that at 0.55. Such a large reduction of the signal from the acid drops opens up the possibility of detecting small backscattering contributions by aerosol species which do not absorp in the infrared.

Sulfur: Its Solubility and Optical Constants

As the remainder of this paper hinges upon the concept that sulfur does not dissolve in sulfuric acid (personal communication, O. B. Toon, Ames Research Center, 1978), we searched the International Critical Tables (ref. 16) and other sources for a quantitative measure of its solubility in the acid. None was found, but Fike (ref. 17) states that the sulfur coatings of concentrated-acid containers were generally unaffected after several years of service. We are indebted to Dr. T. W. Scattergood of SUNY-Stonybrook, who performed the following experiment and observations for us.

An amount of chemically pure, powdered sulfur (sublimed) equal to 2.8 mg was dropped into 250 ml of aqueous solution which was 88% H_2SO_4 by weight. The sulfur, despite its slightly greater density, stayed on top of the solution until it was dispersed throughout by mechanical stirring. The sulfur did not appear to be readily wetted by the acid. In about 1 day much of it had settled to the bottom of the beaker although some still remained on the surface. After 15 days at room temperature the distribution of sulfur powder was about the same, and less than about one fifth of it by visual estimate had disappeared. Thus an upper limit on the mass of the sulfur that dissolved in the 88% acid solution during 15 days was 1.3 parts per million. This limit may be uncertain by a factor of 2 because of the method of visual estimation employed. This experiment, together with the observation by Fike (ref. 17), provides a factual basis for the calculations of inhomogeneous models of the Venus clouds which follow.

The optical constants of sulfur in the infrared are required to evaluate these inhomogeneous models, so we now describe how they were obtained. As will be shown, the dependence on their exact value is not strong.

Although the constants are well determined at 0.5893 μm (ref. 18, p. E-219) they are relatively unknown at other wavelengths. However, spectra of orthorhombic sulfur, S_8, have been obtained from 0.1 to 200 μm by several authors. In particular, spectra from Nyquist and Kagel (ref. 19), Khare and Sagan (ref. 20), the Thermophysical Properties of Matter (ref. 21), and MacNeil (ref. 22) are free of all absorption features (other than those of expected contaminants) between 2 and 7 μm, and the nearest strong sulfur absorption is at 11.8 μm. Thus, we feel confident that the imaginary index near 3.4 μm is quite small. MacNeil estimated from her transmission spectra that the exponential absorption coefficient α, between 2 and 10 μm, was about 4 cm^{-1}. Hence, we use

$$n_i = \frac{\alpha\lambda}{4\pi} \sim 10^{-4}\left(\frac{\lambda}{3.4}\right)$$

with λ in μm.

For the real part of the refractive index, normal dispersion can be assumed because absorption has been shown to be negligible. As we are also far removed from strong absorption features, we need employ only the first two terms of Sellmeyer's equation (ref. 23, p. 96) to calculate the real index to the accuracy we require. Thus we use

$$n_r^2 = 1 + \frac{B\lambda^2}{\lambda^2 - \lambda_0^2}. \tag{28}$$

with B determined from the known index at 0.5893 μm, and the fundamental wavelength $\lambda_0 = 0.13$ μm from Cook and Spear (ref. 24). This gives $n_r = 1.96$ at 3.4 μm. MacNeil (ref. 22) calculated a reflectivity of 0.075 between 2 and 10 μm for one surface of a single crystal, which requires $n_r = 1.75$ to satisfy the equation for reflection at normal incidence $[(n - 1)^2/(n + 1)^2]$. Noting that the dielectric constant of orthorhombic sulfur = 4.0 (ref. 18), we select a value for n_r of 1.80 at 3.4 μm. Young (ref. 1) states that the real index of his sulfur particles is 1.9 (presumably at 0.9 μm, the wavelength of the Venera 9 and 10 nephelometers).

Inhomogeneous-Drop Model

The Mie theory for single scattering by an inhomogeneous drop was first worked out by Aden and Kerker (ref. 25) and by Guttler (ref. 26). Recently, Wickramasinghe (ref. 27) has reformulated the equations for inhomogeneous Mie coefficients in a more explicit manner, although we note that a printing error has nearly obliterated a minus sign before the first term of the second line of his equation (3.45). As Kerker (ref. 8) noted, the variety of numerical calculations that might be explored with the inhomogeneous drop model is immense because the size parameter and refractive index of both the core and coating are variable parameters. Although he considered many examples, Kerker did not treat the one applicable to the suggestion of sulfur in the Venus clouds.

Consider an inhomogeneous drop (fig. 8) containing a spherical, homogeneous core of radius R_o and complex index m_1, surrounded by a concentric coating of outer radius R and index m_2. For the example of sulfur coated by H_2SO_4 this model describes at 3.4 μm a transparent dielectric core surrounded by a strongly absorbing dielectric coating. In the specific case of Venus, the visible polarization observations set the effective outer radius R at about 1 μm. Thus, only the core radius R_o remains as a variable parameter.

There are at least four different ways, however, in which R_o can vary relative to R as the integration over the particle size distribution is performed. In most cases, the core-size dependence on R can be written as

$$R_o = CR^{(p+1)} \qquad -1 \le p \tag{29}$$

where C is a constant. In the first case, $p = -1$ so that R_o remains constant throughout the size distribution; particles in the distribution smaller than C are entirely homogeneous core material, with coating applied only to drops larger than C. In the second case, $p = 0$, so that R_o scales as a fixed fraction of R throughout the distribution. We call this the scaled-core model. In a third case, $p > 0$, hence R_o grows faster than R across the size distribution and will eventually equal R, say at some value V. In this case, $C = V^{-p}$, and particles larger than V are entirely core material; we call this the growing-core model. A fourth case, which we shall call the constant coating model, has a constant thickness t of liquid coating the core in those drops large enough to contain a core, that is, where $R > t$. For $R < t$, the drops are entirely liquid material. To describe this model, equation (29) is modified slightly so that $R_o = R - t$. We note that for small values of t this model has the same core-size dependence on R as does the scaled-core model, that is $p = 0$ and $C = 1$.

New Mie coefficients must be employed to describe the inhomogeneous drop. Once they have been obtained, the calculation proceeds as in the homogeneous model. Equations for the required coefficients are given, for instance, by Kerker (ref. 8, pp. 189-195) and Wickramasinghe (ref. 27, pp. 29-31). Rather than reproduce them here, suffice it to say that we have evaluated them for the first three orders.

We have not attempted to derive a general recurrence relation for the inhomogeneous Mie coefficients because in most cases they need to be used only in the first few terms of the series for the phase function and efficiency factors. The remaining terms can be obtained in the usual manner from homogeneous coefficients. The reason for this follows from the concept of ray localization for $x > 1$. According to this principle, the nth term in each series corresponds to the contribution from the light ray that passes the drop at a distance, mr, of $n\lambda/2\pi$ from its center (fig. 8). Thus, terms where n is less than $2\pi m_2 R_o/\lambda$ are strongly influenced by the core material and must be calculated from inhomogeneous Mie coefficients. Higher order terms correspond to rays that miss the core; they can be calculated from the homogeneous model. Thus it will be useful to define an inhomogeneous drop parameter, nI, to indicate how many inhomogeneous coefficients are required. For the specific case of Venus at 3.4 μm,

$$nI \equiv |z_{core}| = \frac{2\pi R_o}{\lambda} |m_1| < |m_2| x = 2.6 \qquad (30)$$

when using Hansen and Hovenier's effective drop radius of 1.05 μm (ref. 3). We shall shortly show that only the first three terms need to be calculated from inhomogeneous Mie coefficients for the narrow particle size distribution of Venus.

In the more general case, the value of nI will depend upon the manner in which R_o scales with R, and also on the width of the particle size distribution. However, by defining $nI = |z_{core}|$ we avoid the difficulty calculating inhomogeneous coefficients described by Kerker (ref. 8, p. 200). In that situation, n was set by the value of R rather than by R_o, which caused $n >> |z_{core}|$ in those Riccati-Bessel functions and derivatives associated with the core as $R_o \to 0$. As mentioned earlier, Kattawar and Plass (ref. 9) found that calculations employing upward recurrence relations are numerically unstable in such a case. Thus, by using inhomogeneous coefficients obtained through upward recurrence only so far as nI, and then using homogeneous coefficients obtained from downward recurrence for the remaining terms, the numerical instability is avoided for most values of R_o/R. A thin film coating on particles with a broad size distribution is an extreme example where it would be desirable to have a general recurrence relation for the inhomogeneous coefficients because of the large value of nI.

The multiple scattering Mie program for planetary reflection (described earlier) was modified to calculate inhomogeneous Mie coefficients through the third order following Wickramasinghe (ref. 27). It was also modified to permit R_o to vary according to equation (29). The inhomogeneous drop program thus created was tested by requiring it to produce the same results as the homogeneous drop calculation to five or more significant figures in four equivalent test cases. The first equivalence test had $m_1 = m_2$ = the index of H_2SO_4, and R_o had a constant value of one half the modal drop radius (or 0.415 μm). The second test case had m_1 = the index of H_2SO_4, $m_2 = 1$, and R_o had a constant value of 4 μm (the size distribution peaks at 0.8 μm). The third test case had m_1 = sulfur, $m_2 = H_2SO_4$, and a scaled core where $R_o = 0.01$ R. It was for such very small cores that Kerker (ref. 8, p. 200) experienced difficulty with upward recurrence as mentioned above. We also calculated his specific case ($\lambda = 2.5$ μm, $m_1 = 2.105\text{-}0$, $m_2 = 1.482\text{-}0$, $x = 10$, $R_o/R = 0.005$, $b = 0.07$) and found no difference from our corresponding homogeneous calculation. In the fourth test, m_1 = sulfur, $m_2 = H_2SO_4$, and the constant coating thickness was 2 μm, a value so large that less than 10^{-3} of the drops had cores.

In a fifth equivalence test the scaled core size was as large as the drop: $R_o = R$, $m_1 = H_2SO_4$, and $m_2 = 1$. This case thoroughly tests the inhomogeneous drop program because three different values of z remain defined throughout the calculation and because $|z_{core}|$ approaches 5 at the large end of the size distribution, thus fully utilizing the higher-order inhomogeneous Mie coefficients. The result of using more inhomogeneous coefficients in this test is clearly shown by the change of the single scattering phase function in figure 9. Other functions, such as the anisotropy parameter, the single-scattering cross section, and the albedo similarly approach the homogeneous result as more

inhomogeneous coefficients are used. Inasmuch as this is an extreme test ($R_o = R$) and the residual deviation is less than 2% after the third inhomogeneous term, we consider $nI = 3$ more than adequate for the Venus calculation.

Finally the inhomogeneous drop program was tested by using it to recalculate the scattering and extinction efficiency factors of inhomogeneous drops published by two other authors. Since theirs were monodisperse calculations, our program was temporarily modified to bypass the particle size integration. In each test when the core radius became so large that $nI > 3$, the test comparison failed significantly, as it should. Espenscheid et al. (ref. 28) calculated a nonabsorbing case where $m_2 = 1.481$, $m_1 = 2.105$, and $x = 10$. They used upward recursion wherever possible (small values of n/z) which may account for the small, but consistent difference of 2/3% between their values of Q_{scat} and ours as R_o/R approached zero. Fenn and Oser (ref. 29) calculated the inverse case to ours, that of an absorbing core ($m_1 = 1.59-0.66i$) covered by a nonabsorbing coat ($m_2 = 1.33$). At values of R_o/R equal to 0.5 and 0.833, with x between 1 and 4, our calculations of Q_s and Q_e agreed with theirs to within our ability to read their graphs (about 4% or better). They also calculated absorption efficiency factors for an absorbing coating ($m_2 = 1.473-0.169i$) with the same absorbing core. At $x = 12.3$ our values of Q_a (obtained from the difference between our calculated values of Q_e and Q_s) at $R_o/R = 0.0273$ and 0.0741 agreed with theirs to 5 significant figures. However, comparison with certain plotted data in Wickramasinghe (ref. 27) and Pilat (ref. 30) produced agreement only on the order of 10%.

We now want to demonstrate the dependence of the reflectivity function on the variable parameters of the inhomogeneous drop. Where the homogeneous drop has five independent parameters, the inhomogeneous drop has eight, as well as the manner in which the core radius varies over the size distribution. For cores that do not occupy the entire drop, it is reasonable to assume that the reflectivity function of the inhomogeneous drop model varies with wavelength, effective radius, variance, and coating index in about the same way as it does for the homogeneous drop; thus we will not demonstrate the dependence on those parameters. Variation of the three additional parameters of the inhomogeneous drop — R_o, and the real and imaginary parts of the core index — can produce a dramatic effect on the reflectivity function depending on their value. However, for cores of sulfur the imaginary index is so small ($\sim 10^{-4}$) that variation of this parameter over a reasonable range has no effect whatever. The real index of sulfur is larger than that of the H_2SO_4 coating, so its variation could be significant. In figure 10 the real part of the core index is varied over the range of possible values (1.75-1.95). It can be seen there that this range of variation does have a noticeable, but small, effect on the reflectivity. The model's sensitivity to this core parameter is much less than it is to the real index of the coating (fig. 3).

We now compare the four previously described ways of varying the core radius during integration over the size distribution. This is done in figure 11 for moderately large cores. Principally because of their smaller volume of absorbing material, the scaled-core and constant-coating models have significantly greater reflectivity than either of the other two models at most phase angles. We noted earlier that for small coating thicknesses both of these models have the same core-size dependence on drop radius ($p = 0$); thus, it is

not surprising that their reflectivities have a similar dependence on phase angle. It is a bit surprising, however, that the magnitude of the reflectivity calculated for these two models is so similar (see also figs. 12 and 13). The constant in equation (29) is a measure of core size for the scaled core model ($= R_o/R$). In the constant coating model $R_o/R = 1 - t/R \cong 1 - t/a$, where we have used $R \cong a$ because of the small width of the size distribution. By comparing figures 12 and 13 it can be seen that as the core increases in size, the two reflectivity functions become nearly equal, and furthermore the two measures of core size also approach equality at $C = 1$. Thus, for large cores, not only do the two models have the same core-size dependence on drop radius, they effectively have the same core size. The narrowness of the size distribution helps produce this effect. The resulting near-equality of the reflectivity functions of the two models is thus not so surprising.

The constant-coating, the scaled-core, and the constant-core models should also be compared (figs. 12, 13, and 14) at the opposite range Ω core-size variation as R_o/R approaches zero. Both the constant-core and scaled-core models regularly approach the homogeneous-model reflectivity function as core size diminishes. However, the reflectivity of the constant-coating model at small phase angles dips somewhat below that of the homogeneous and scaled-core models when R_o/R is <0.33. This small enhanced absorption occurs when the constant coating thickness is approximately one-fourth the wavelength.

The growing core in figure 11 is described by $R_o = R^2/(2\ \mu m)$, so that $R_o = R$ at 2 μm. For convenience in doing this particular calculation, the size distribution was cut off at 2 μm where its value is more than three orders of magnitude below the peak value. We note that the reflectivity of the growing core model has a steeper slope than the other three models because the larger drops become relatively less absorbing than the smaller ones. The reflectivity of the constant core example has an intermediate slope. Although these differences are noticeable, they are much smaller than those due to changing core size.

Regardless of the mode of variation of the core radius, the reflectivity function is most sensitive simply to the effective size of the core itself. This strong sensitivity is clearly shown in figures 12-14, and is based on the greater volume of highly reflecting, nonabsorbing material in the larger cores. When R_o/R is greater than 0.5, this sensitivity is particularly strong, and the reflectivities of the scaled-core and constant-coating models are nearly equal, as noted above. In those models, both the level and the slope of the reflectivity function change rapidly for $R_o/R > 0.7$. Finally, drops with cores $\leq 0.1\ R$ are nearly indistinguishable from homogeneous particles, with the small variation of the constant-coating model noted before being the only exception.

Inhomogeneous-Cloud Model

If large particles of elemental sulfur are hidden at large visual optical depths as suggested by Young (ref. 1), then they might be detected in the infrared because a small percentage of them could be brought up to the level of the 3.4 μm observations by convective overshoot or other turbulent

processes. There the particles would be particularly noticeable because absorption in the acid drops has already reduced the amount of scattered light. A small contribution to the scattering by nonabsorbing particles should be easily detected, particularly so in the intermediate backscatter directions where the droplet attenuation is strongest. Because both the large size (~13 μm) and the irregular shape of the postulated sulfur particles enhance the infrared backscatter relative to that of acid drops, these characteristics would further assist sulfur particle detection.

Since most infrared observers do not resolve planetary detail, we must consider the postulated sulfur particles to have a uniform horizontal distribution in spite of the known ultraviolet contrasts. We also assume that they have a uniform vertical distribution within the top few optical depths for reasons of mathematical convenience. Hence, in this first approximation we consider a uniform cloud of proposed sulfur particles that is well mixed with the H_2SO_4 cloud drops. A bimodal particle size distribution describes this situation quite well because the inhomogeneity in particle size, indices of refraction, and number density have at least as large an effect upon the planet's backscatter as does its spatial inhomogeneity. Thus we modify the homogeneous model described earlier to include sulfur simply by replacing the existing unimodal size distribution with a bimodal one that has H_2SO_4 drops in the main peak near 1 μm and irregularly shaped sulfur particles in a second, smaller peak near 12 μm. A more general treatment in which the size distributions overlap is also possible, but is not called for by either the quality of current data or the hypothesis of Young's model.

To modify the homogeneous model to incorporate sulfur particles we replace equation (25) by

$$n_B(r) = F_1 n(r,a_1,b_1) + F_2 n(r,a_2,b_2) \tag{31}$$

where $n(r,a,b)$ is given by equation (25) and $F_1 + F_2 = 1$. Here F_1 is the fraction of the total number of particles (acid drops plus sulfur) in the sulfuric acid peak at a_1, and F_2 is the fraction of all particles in the sulfur peak at a_2. The effective radii and effective variances a_1, a_2, b_1, and b_2 are defined by equations (26) and (27) for the two different modes by considering the limits of integration, r_{min} and r_{max}, to separate the particles into two complete and exclusive distributions. In practice, however, a_1, a_2, b_1, and b_2 are variable parameters.

Following equations (23) and (24), the size-integrated phase function and cross sections become

$$P_{(\theta)}^{11} = \frac{\lambda^2 F_1}{2\pi k_s} \int_{r_{min}}^{r_o} [|S_1(r,\theta)|^2 + |S_2(r,\theta)|^2] n(r,a_1,b_1) dr$$

$$+ \frac{\lambda^2 F_2}{2\pi k_s} \int_{r_o}^{r_{max}} [|S_1(r,\theta)|^2 + |S_2(r,\theta)|^2] n(r,a_2,b_2) dr \qquad (32)$$

$$k_{s_e} = F_1 \int_{r_{min}}^{r_o} \sigma_{s_e}(r) n(r,a_1,b_1) dr + F_2 \int_{r_o}^{r_{max}} \sigma_{s_e}(r) n(r,a_2,b_2) dr \qquad (33)$$

(The numbers 1 and 2 within the brackets of equation (32) do not refer to the bimodal distribution; see eqs. (19) and (20).) Here r_o is an intermediate integration limit where we change <u>both</u> the particle shape and the index of refraction to values appropriate to those of solid, irregular sulfur particles. As already mentioned, our treatment of the bimodal distribution as completely separable is a simplification allowed by the state of current theory and data. It will be shown later that this scattering solution is quite insensitive to values of r_o between 3 and 7 μm. A more general treatment would merely require a different integral.

At the temperature of the Venus cloud top (~240 K), elemental sulfur can be expected to be frozen and thus have an irregular shape. The scattering behavior of irregular (nonspherical) particles of size somewhat larger than the wavelength differs systematically from that predicted by Mie theory. In particular, a much smaller peak is seen in the directly backward direction ($\phi = 0$) and the scattering over intermediate backscatter angles is more uniformly distributed. Cuzzi and Pollack (ref. 31) describe a semi-empirical method for obtaining the single scattering phase function and albedo of irregular particles given the Mie values for a set of equal volume spheres of the same refractive index. Their method uses a combination of physical and geometrical optics, and relies on comparison of parameterized phase functions with laboratory observations of the scattering by irregular particles of various sizes and shapes. The semi-empirical theory fits these observations quite well with variation of only two parameters. The first is the size parameter, $x_o = 2\pi r_o/\lambda$, where the transition from Mie scattering by spheres to irregular particle scattering occurs. The second, FTB, is the slope of a straight line representing the angular dependence of that fraction of the scattered light that has been transmitted through the particle. Cuzzi and Pollack (ref. 31) have shown that values of these parameters characterizing a wide range of particle shapes do not vary so widely that "typical" values may not be chosen. Thus, we have used their semi-empirical theory with $x_o = 7 (r_o = 3.8$ μm), a value characteristic of large particles, in our

calculation of the scattering by the sulfur mode of the bimodal distribution. In demonstrating and testing our calculations we have used FTB = 1.5, characteristic of cubes. However, a value of 3 is physically more reasonable for large polyhedra, and we use that value later to set observational limits on other parameters.

The modifications just described were tested by several reductions to known cases. First, using only a unimodal size distribution (a = 1.05 μm, b = 0.07), the spherical-drop part of the program was shown to reduce to the H_2SO_4 homogeneous drop, homogeneous cloud model reflectivity function at 1 μm (Case No. 3 of Hansen and Travis, ref. 6) and at 3.65 μm by setting x_o very large (equal to 99). Still using a unimodal size distribution, the irregular-particle part of the program was checked by requiring it to reproduce a previously calculated phase function at $\lambda = 3.71$ cm when the value of x_o fell near the center of the range of integration. This calculation was related to laboratory observations of the scattering of microwaves by particles with size parameters similar to ours (fig. 5 of Cuzzi and Pollack, ref. 31). The bimodal distribution was tested in two separate cases by requiring it to reduce to the 3.65 μm absolute reflectivity function of the homogeneous model calculated earlier. In the first case, the second peak was simply eliminated ($F_2 = 0$). In the second case, the first peak was eliminated ($F_1 = 0$) and the second peak converted to H_2SO_4 spheres ($x_o = 99$) located at 1.05 μm ($a_2 = 1.05$ μm). In tests where previous calculations were reproduced, the agreement was good to five or more significant figures. In reproducing Case No. 3 of Hansen and Travis (ref. 6), the agreement was as good as our ability to read their figure 27 (about 3%).

We will now discuss the dependence of the reflectivity function on the variable parameters of this inhomogeneous cloud model and point out those that are the most significant. Since the fraction of all particles in the second (sulfur) mode that we may expect to see at 3.4 μm will probably be less than the 1% suggested by Young (ref. 1), it is reasonable to assume that this model will have a dependence on the parameters of the sulfuric acid droplet mode similar to that of the homogeneous model. In addition to those five parameters, the inhomogeneous cloud model presents seven more to consider. As with the inhomogeneous drop model, the dependence on the imaginary index of sulfur is negligible because its value is so small in the first place. The dependence of the inhomogeneous cloud model on the real index of sulfur (fig. 15) was also found to be negligible. It was mentioned earlier that because the modes of the size distribution were separate, the dependence on x_o was small for r_o in the range between 3 and 7 μm. Of course outside that range, the sensitivity to x_o can be appreciable because inappropriate shape and index changes are being made on the shoulder of one mode or the other. These effects can be seen in figure 16 where r_o is varied from 1.6 to 11.5 μm. Unless stated otherwise, all succeeding calculations were made with $r_o = 3.8$ μm ($x_o = 7$). The inhomogeneous cloud model is not as sensitive to FTB, the slope of the parameterized phase function of the transmitted light, as might have been expected. Figure 17 shows, however, that the dependence does occur where expected, at the largest backscatter angles, because the transmitted component dominates at large scattering angles when FTB is small. The models' dependence on the effective variance of the sulfur peak, shown in figure 18, is also small. Backscattering increases slightly with decreasing variance because the

"standard" size distribution employed here is asymmetric and narrowing the second mode creates proportionally more particles with larger radii.

The backscatter ($\phi \leq 70°$) of the inhomogeneous cloud model is most sensitive to two parameters: the effective radius of the sulfur particles, a_2, and the fraction of all particles in the sulfur mode, F_2. As will be shown in the next section this strong sensitivity, depicted in figures 19 and 20, results from a nearly linear dependence of the model's backscattered reflectivity on the total area of large particles. Thus curves with about the same reflectivity at $\phi = 20°$ are nearly identical, regardless of whether the varied parameter was a_2 or F_2. The range of F_2 shown in figure 20 is from zero to 1/100, which spans the range from a homogeneous model to an inhomogeneous model containing as much sulfur as was proposed by Young (ref. 1). It is clear from this figure that the backscattering of the inhomogeneous cloud model is sensitive to only a few percent of the proposed amount of sulfur.

COMPARISON AND DISCUSSION OF MODELS

Backscatter Dependence on the Sulfur Volume or Area

In the preceding section we found that although there can be many parameters associated with the different inhomogeneous models, there are only a few that really govern the shape and level of the reflectivity function. We shall call these the principal parameters of each model; they are listed below. The first three in each model refer to sulfuric acid drops.

Homogeneous model	a, n_r, n_i
Inhomogeneous drop	a, n_r, n_i, R_o
Inhomogeneous cloud	a_1, n_r, n_i, a_2, F_2

The reflectivity function of the homogeneous model has a broad minimum near a phase angle of 30° (fig. 7); hence that is a region where scattering associated with the additional principal parameters of the inhomogeneous models will be most apparent. Accordingly, we investigate the dependence of the backscattered light on R_o, a_2, and F_2 at two backscattering phase angles: $\phi_B = 20°$ and $\phi_B = 40°$.

In figure 21 we have plotted the reflectivity at ϕ_B of both the scaled-core and constant-core inhomogeneous drop models versus core volume. We used a core volume $4/3\pi(aR_o/R)^3$ employing the effective radius a of the size distribution. Using the mean or modal radii increases the slope of the curves but does not otherwise change the results. It is clear from the figure that the backscattering of the constant-core model has a highly linear dependence on the sulfur core volume which can be expressed as

$$\tilde{R}(3.4,\ \phi_B = 20°,\ 40°) = 0.0436(R_o/R)^3 + 0.00774 \qquad (34)$$

The difference between the backscatter at 20° and 40° is negligible so averages have been used in equation (34). It can also be shown that the backscatter has a similar, but inverse dependence, on the volume of H_2SO_4. Thus, we conclude that it is primarily the volume of absorbing coating that depresses the backscatter and causes the reflectivity function to be as steep as it is.

It is quite apparent in figure 21 that backscattering by the scaled-core model is not linearly dependent on volume, having a much stronger dependence than that for $R_o \gtrsim 0.4R$. The constant-coating model produces a nearly identical plot of $\tilde{R}$ versus volume because for large cores it has the same dependence of core size on drop radius as does the scaled-core model, as noted earlier. The difference between the constant-core model and these other two models probably arises from the fact that the constant-core model has a constant volume of sulfur at each fractional size level, whereas the other two models have a variable volume of sulfur through the integration over particle size. Since the backscatter is proportional to sulfur volume, the size integration permits the larger fractional cores to dominate the reflectivity of the scaled-core and constant-coating models.

We noted earlier that the sensitivity of the inhomogeneous-cloud reflectivity function to both F_2 and a_2 was due to its dependence on the total area of sulfur particles. The inhomogeneous cloud reflectivity function versus both parameters is plotted in figure 22 (the upper four curves). The nearly linear dependence on F_2 can be expressed by

$$\tilde{R}(3.4,\ \phi_B = 20° \text{ to } 40°) \cong 20.8\ F_2 + 0.00774\ , \qquad \text{with } a_2 = 12\ \mu m \tag{35}$$

and the dependence on a_2 (in microns) by

$$\tilde{R}(3.4,\ \phi_B = 20° \text{ to } 40°) \cong 4.42\times10^{-5}(a_2)^2 + 0.00774\ , \qquad \text{with } F_2 = 3.2\times10^{-4} \tag{36}$$

Again, the difference in backscatter between 20° and 40° is so small that averages have been used to obtain these equations. To determine these relations, we found that in the computer calculation the integration over particle size had to be carried to very large values (x = 85) to get all the backscattered light. As in previous calculations of this model, we have used FTB = 1.5 for demonstration purposes. Because this may be physically unreal (large particles do not often have square corners), we have also calculated $\tilde{R}$ as a function of F_2 with FTB = 4. These are the lowest two curves in figure 22. Increasing FTB reduces the slope of the dependence on F_2, but does not remove the dependence or its linearity. These results are all consistent with the observation that non-absorbing, high-index particles that are considerably larger than the wavelength are good reflectors, and the reflection is proportional to the total area of the reflector.

Comparison of Models

Similarities- All three models are similar in that at 3.4 μm they have no glory or rainbows as ϕ approaches zero. The homogeneous model produces only

a small monotonic increase of ~7% in $\tilde{R}$ as ϕ decreases from 40° to 0.5°. The inhomogeneous models have an even smaller increase. This result is consistent with most of the particles being considerably smaller than the wavelength. Both inhomogeneous models are similar in that variation of any of the "inhomogeneous" parameters changes the backscattering more than the forward scattering because the forward scatter is due principally to diffraction by the abundant H_2SO_4 drops. Variation of R_o in the inhomogeneous drop (up to values of about 0.6R) produces changes in the scattering that are somewhat similar to those produced by changing either n_r or n_i of the acid in the homogeneous model. This happens because the sulfur volume determines the volume of acid remaining in the drop. Thus, small sulfur cores could have an effect on 3.4-μm observations similar to a reduced concentration of the acid. Fortunately the wavelength dependence of an H_2O-H_2SO_4 solution is sufficiently different from that of an S-H_2SO_4 mixture that large errors in the deduced concentration are not possible when observational spectra covering both liquid H_2O and H_2SO_4 bands are analyzed.

Differences- Variation of the radius of the acid drops of the homogeneous model affects the 3.4 μm reflectivity function in a manner which is distinctly different from that due to varying other parameters of the same or different models. (Compare fig. 5 with figs. 14 and 20, for example.) Such changes are predictable. First, as the particles become small compared to λ the $\tilde{R}$ tends toward an isotropic distribution similar to Rayleigh scattering. Second, as the particles approach λ in size, diffraction enhances forward scattering while absorption within the particles reduces the backscatter, resulting in a very steep reflectivity function.

In figure 23 we contrast the effects of varying the other principal parameters of the three models. Variation of F_2 and a_2 of the inhomogeneous cloud model changes the shape of the reflectivity function through a purely backscattered enhancement; varying R_o of the sulfur core, or n_r or n_i of the acid, primarily affect the overall level of the curve. In summary the large, non-absorbing, high-index particles in the second mode of the inhomogeneous cloud act roughly like an isotropic reflection added to the droplet scattering, while the volume of non-absorbing core inside the inhomogeneous drops affects the overall level of the reflectivity function by excluding the sulfuric acid absorber.

The Detectability of Sulfur

Minimum detectable amounts of sulfur can be set by comparison of inhomogeneous reflectivity functions with that of the homogeneous acid drop. But to do that, the ratio of the mass density of elemental sulfur to that of a specified concentration of sulfuric acid first must be evaluated. We will use an 85% concentrated solution with a density of 1.71 gm/cm^3, and note that the density falls by less than 5% if a 75% concentrated solution were used. The major uncertainty in the mass density ratio arises from the unknown molecular form of elemental sulfur on Venus. However, Meyer (ref. 32) lists in his table 3.1 the density of nine different allotropes of sulfur (ranging from S_6 to S_∞) and shows that they vary from 1.94 to 2.21 gm/cm^3, a range of only

13%. Thus we pick a middle value of 2.1 gm/cm^3 which produces a value for the S/H_2SO_4 mass density ratio of 1.23 with an uncertainty of ±8%.

Detectability of sulfur in the Venus clouds, in the sense that we shall use it, refers to the ability to observe an enhancement of the 3.4 μm backscattering relative to that calculated for a homogeneous drop. For example, figure 24 shows a band 25% higher than the homogeneous drop reflectivity function. Just within that band lie back scattered reflectivities of inhomogeneous drop models with scaled core radii as large as 0.38 R, and inhomogeneous cloud reflectivities with $F_2 = 0.75\times10^{-4}$. Thus, 3.4 μm observations at $\phi < 100°$ with total (absolute plus internal) errors ≤25% could distinguish the homogeneous model from those inhomogeneous drop models whose scaled core radii were >0.38 R. Because 25% error bars placed upon those curves with $R_o < 0.38$ R would include the homogeneous curve, such observations could not distinguish, hence could not detect, inhomogeneous drops with cores smaller than 0.38 R. Similarly, figure 24 indicates that ±25% total-error observations at $\phi_B = 20°$ to 40° could distinguish the homogeneous model from inhomogeneous cloud reflectivities where $F_2 \geq 0.75\times10^{-4}$ (with $a_2 = 12$ μm, FTB = 1.5).

The ratio of the detectable mass of sulfur m_S to that of H_2SO_4 solution $m_{H_2SO_4}$ can be directly related to the minimum distinguishable values of F_2 or R_o/R set by the total error of the observations. This is particularly simple for the scaled core inhomogeneous drop model where the ratio of the total volume of sulfur (V_S) in the atmosphere to the total H_2SO_4 volume ($V_{H_2SO_4}$) is the same as it is in each drop because there is a core of fixed fractional size in every drop. Thus,

$$\frac{V_S}{V_{H_2SO_4}} = \frac{R_o^3}{R^3 - R_o^3} = \frac{1}{(R/R_o)^3 - 1} \tag{37}$$

and so the minimum detectable mass ratio for inhomogeneous drops is

$$A_{mid} \equiv \left.\frac{m_S}{m_{H_2SO_4}}\right|_{drops} = \frac{\rho_S V_S}{\rho_{H_2SO_4} V_{H_2SO_4}} = \frac{1.23}{(R/R_o)^3 - 1} \tag{38}$$

where we have used a density ratio $\rho_S/\rho_{H_2SO_4} = 1.23$ as discussed earlier. For the inhomogeneous cloud model, the minimum detectable mass ratio is

$$A_{mic} \equiv \left.\frac{m_S}{m_{H_2SO_4}}\right|_{clouds} \cong \frac{\rho_S a_2^3 N_S}{\rho_{H_2SO_4} a_1^3 N_{H_2SO_4}} = 1.23\left(\frac{a_2}{1.05}\right)^3 F_2 \tag{39}$$

since $N_S/N_{H_2SO_4} = F_2$ and we consider a_1 to be specified by the work of Hansen and Hovenier (ref. 3).

To take the case from figure 24 as an example, inserting $R/R_o = (0.38)^{-1}$ into equation (38) gives A_{mid} equal to 7.1% for the inhomogeneous drop. That is, 25% or better observations could tell inhomogeneous drops with more than 7.1% sulfur from homogeneous acid drops. More accurate evaluation of R_o could be made by referring to plots of $\tilde{R}$ versus volume, such as figure 21, but that is not necessary at this point.

The inhomogeneous cloud model has two unspecified parameters, a_2 and F_2. Young (ref. 1) has proposed that $a_2 \geq 10a_1$, so we will evaluate equation (39) at two values of a_2: 9 μm and 18 μm. As mentioned earlier, values of FTB = 1.5 may be unreal for large particles, so we use now a value of 3 appropriate for large polyhedra. This is consistent with the shape of the double pyramid habit of orthorhombic sulfur shown by Adams and Spear (ref. 33). Because of the high sensitivity of the back scattered reflectivity to F_2, it is both impractical and inaccurate to evaluate the minimum distinguishable (detectable) value of F_2 from families of curves such as those in figure 20. Since $\tilde{R}$ is directly proportional to F_2, the minimum distinguishable value can be extrapolated from a linear plot as shown in figure 25 for $a_2 = 18$ μm. Again we note that the difference between $\phi = 20°$ and 40° is small enough to permit averaging, so that if $a_2 = 18$ μm we find from the figure that the minimum distinguishable value of F_2 is 6.1×10^{-5} at the ±25% total-error level. It is of course proportionately smaller at the ±15% error level. Similar calculations for $a_2 = 9$ μm give the minimum distinguishable value of F_2 as 2.2×10^{-4} at the ±25% error level. Thus, depending on the size of the postulated sulfur particles we expect that their minimum number density detectable by ±25% total-error observations at ϕ_B is between 6×10^{-5} and 22×10^{-5} times the number density of acid drops. This is about two orders of magnitude smaller than that proposed by Young and indicates the sensitivity of back-scattered infrared observations. We note that such observations pertain to the first 3.4 μm optical depth within the cloud, that is, to the upper part of the cloud.

The small value for the minimum detectable number density becomes a large value of minimum detectable mass because these particles are so large. Even so, it is still interesting to compare the minimum detectable amounts of sulfur for both inhomogeneous models. Evaluating equation (39) at the ±25% level with the values of F_2 determined above, we find that the minimum detectable mass of sulfur in the inhomogeneous cloud model ranges from 17% of the mass of acid for 9 μm particles to 38% for 18 μm particles, as compared to 7% of the mass of acid if the sulfur is within each drop.

Penetration Height of 3.4 μm Observations

Finally we estimate the height above the surface of Venus to which these 3.4 μm observations and minimum detectable masses pertain. We define the effective extinction cross section or coefficient as

$$\text{eff.}k_e(\lambda) = (1 - \overline{\cos\theta})k_s(\lambda) + k_a(\lambda) \qquad (40)$$

where $\overline{\cos\theta}$ is the anisotropy factor (ref. 6). This definition differs from that of Lacis (ref. 34, figure 2) in that we apply the correction for forward

scattering $(1 - \overline{\cos\theta})$ only to k_s rather than to the sum of $k_s + k_a$ as did Lacis. Because both the visible polarization and the 3.4 μm observations pertain primarily to single scattered light, we can write

$$1 \simeq \frac{\tau_{eff.IR}}{\tau_{eff.VIS}} = \frac{\int_{h_{IR}}^{\infty} eff.k_e(IR)\, N(h) \sec z\, dh}{\int_{h_{VIS}}^{\infty} eff.k_e(VIS)\, N(h) \sec z\, dh} \tag{41}$$

Assuming that $eff.k_e \sec z$ is independent of height gives

$$\int_{h_{IR}}^{\infty} N(h)dh \simeq \frac{eff.k_e(VIS)}{eff.k_e(IR)} \int_{h_{VIS}}^{\infty} N(h)dh \tag{42}$$

Here $N(h)$ is the number density at height h, and h_{IR} and h_{VIS} are the deepest heights from which radiation of the wavelength specified has arisen when $\tau_{eff.}$ is large.

The column density integral on the right side of equation (42) was determined graphically from the density model of Lacis (ref. 34, fig. 8) with $h_{VIS} = 66.5$ km. The effective extinction cross sections were calculated at 0.55 and 3.4 μm using the homogeneous model of H_2SO_4 drops at 84-1/2% concentration and 300 K temperature. Equation (42) was then evaluated graphically and produced a value for h_{IR} of 67.5 km. We note that Lacis' density model is sufficiently steep at this height that a factor of two reduction in the 3.4 μm effective extinction cross section (which would result from use of Lacis' definition) would cause only a 2-km increase in depth. Thus we conclude that the 3.4 μm observations pertain to about the same height as those in the visual, or to just slightly higher.

SUMMARY AND CONCLUSION

The ability to detect small contributions to the scattering of sunlight by sulfur or other nonabsorbing species is greatly enhanced in the infrared absorption band of sulfuric acid where absorption reduces backscattering by the numerous homogeneous acid drops to levels more than 40 times below those in the visual.

A planetary reflectivity function, whose shape is quite similar to that of the single scattering phase function with strong absorption, has been defined and related to other known functions.

Two inhomogeneous models containing sulfur have been described and tested. The principal new parameters associated with these inhomogeneous models are the radius R_o of the sulfur core within an inhomogeneous drop, and the effective radius a_2 and relative number density F_2 of large sulfur particles in the inhomogeneous cloud model. A core-size parameter, nI, indicating how many inhomogeneous Mie coefficients are required has been defined for the inhomogeneous drop model. Calculations with these models at 3.4 μm show that backscattering near phase angles of 30° by the constant core, inhomogeneous drop model has a linear dependence on core volume (R_o^3); backscatter from the inhomogeneous cloud model has a linear dependence on the total area of large sulfur particles through either $(a_2)^2$ or F_2. The volume of non-absorbing core inside the inhomogeneous drop affects the overall level of the 3.4 μm reflectivity function by excluding the sulfuric acid absorber; in contrast, the area of the large, non-absorbing, high-index sulfur particles affects the shape of the reflectivity function by adding a nearly isotropic reflection to the steep curve of the acid drops.

Minimum detectable amounts of sulfur are based on the ability to observe an enhancement of the 3.4 μm backscatter relative to that calculated from the homogeneous model. Observations with ±25% or less total error could distinguish the homogeneous drop reflectivity function from that of inhomogeneous drops if $R_o \geq 0.4R$. Similarly, ±25% observations could distinguish the inhomogeneous cloud reflectivity function of sulfur particles with effective radii between 9 and 18 μm if $F_2 \geq 22\times10^{-5}$ or 6×10^{-5}, respectively. These minimum distinguishable parameters lead to ratios of the minimum detectable mass of sulfur to that of H_2SO_4 for the inhomogeneous drop model of 7%, and for the inhomogeneous cloud model of 17% or 38%, depending on particle size.

These calculations lead us to conclude that moderately accurate 3.4 μm observations of the intermediate angle backscatter from Venus are capable of detecting quite small amounts of elemental sulfur at heights above the planetary surface comparable to those of the visual observations.

REFERENCES

1. Young, Andrew T.: An Improved Venus Cloud Model. Icarus, vol. 32, Sept. 1977, pp. 1-26.

2. Hapke, Bruce; Nelson, Robert; Woodman, J. H.; and Barker, E. S.: UV Spectroscopy of Venus: Evidence for an Elemental Sulfur Component of the Clouds. Bull. Am. Astron. Soc., vol. 6, 1974, pp. 368-369.

3. Hansen, James E.; and Hovenier, J. W.: Interpretation of the Polarization of Venus. J. Atmos. Sci., vol. 31, no. 4, 1974, pp. 1137-1160.

4. Pollack, James B.; Strecker, Donald W.; et al.: Properties of the Clouds of Venus as Inferred from Airborne Observations of its Near-Infrared Reflectivity Spectrum. Icarus, vol. 34, 1978, pp. 28-45.

5. Irvine, William M.; Simon, Theodore; et al.: Multicolor Photoelectric Photometry of the Brighter Planets. III. Observations from Boyden Observatory. Astron. J., vol. 73, no. 9, 1968, pp. 809-810 and 817-818.

6. Hansen, James E.; and Travis, Larry D.: Light Scattering in Planetary Atmospheres. Space Sci. Rev., vol. 16, no. 4, Oct. 1974, pp. 527-610.

7. van de Hulst, Hendrik: Light Scattering by Small Particles. Wiley, New York, 1957.

8. Kerker, M.: The Scattering of Light and Other Electromagnetic Radiation. Academic Press, New York, 1969.

9. Kattawar, George W.; and Plass, Gilbert N.: Electromagnetic Scattering from Absorbing Spheres. Appl. Opt., vol, 6, Aug. 1967, pp. 1377-1382.

10. Hansen, James E.: Multiple Scattering of Polarized Light in Planetary Atmospheres. Part II. Sunlight Reflected by Terrestrial Water Clouds. J. Atmos. Sci., vol. 28, 1971, pp. 1400-1426.

11. Stokes, George G.: On the Intensity of Light Reflected from or Transmitted Through a Pile of Plates. Proc. Roy. Soc. (London), vol. 11, 1862, pp. 545-556.

12. Pollack, James B.; Erickson, Edwin F.; et al.: Aircraft Observations of Venus' Near-Infrared Reflected Spectrum: Implications for Cloud Composition. Icarus, vol. 23, 1974, pp. 8-26.

13. Palmer, Kent F.; and Williams, Dudley: Optical Constants of Sulfuric Acid; Application to the Clouds of Venus? Appl. Opt., vol. 14, 1975, pp. 208-219.

14. Jones, A. Daniel: Optical Constants of Sulfuric Acid in the Far Infrared. J. Quant. Spectrosc. Radiat. Transfer., vol. 16, no. 12, 1976, pp. 1017-1019.

15. Boese, Robert W.; Miller, Jacob H.; and Inn, Edward C. Y.: Intensity Measurements of the 1 μm CO_2 Bands. J. Quant. Spectrosc. Radiat. Transfer., vol. 6, 1966, pp. 717-725.

16. Washburn, E. W., ed.: International Critical Tables. Vols. I-III. McGraw-Hill, New York, 1926-1933.

17. Fike, Harold L.: Sulphur Research Trends. Advances in Chemistry Series, R. F. Gould, ed., vol. 110, ACS, Washington, D.C., 1972, p. 17.

18. Weast, R. C., ed.: Handbook of Chemistry and Physics. Fifty-eighth ed., CRC Press, Cleveland, 1977, p. E-219.

19. Nyquist, Richard A.; and Kagel, Ronald O.: Infrared Spectra of Inorganic Compounds (3800 - 45 cm^{-1}). Academic Press, New York, 1971, pp. 254-255.

20. Khare, B. N.; and Sagan, Carl: Cyclic Octatomic Sulfur: A Possible Infrared and Visible Chromophore in the Clouds of Jupiter. Science, vol. 189, 1975, pp. 722-723.

21. Touloukian, Y. S.; and DeWitt, D. P., eds.: Thermal Radiative Properties of Nonmetallic Solids. Vol. 8. Thermophysical Properties of Matter, IFI/Plenum, New York, 1972, pp. 116-117.

22. MacNeill, Catherine: Infrared Transmittance of Rhombic Sulfur. J. Opt. Soc. America, vol. 53, no. 3, 1963, pp. 398-399.

23. Born, Max; and Wolf, Emil: Principles of Optics: Electromagnetic Theory of Propagation, Interference, and Diffraction of Light. Second ed. Pergamon Press, Macmillan Co., New York, 1964.

24. Cook, B. E.; and Spear, W. E.: The Optical Properties of Orthorhombic Sulfur Crystals in the Vacuum Ultraviolet. J. Phys. Chem. Solids, vol. 30, 1969, pp. 1125-1134.

25. Aden, Arthur L.; and Kerker, Milton: Scattering of Electromagnetic Waves from Two Concentric Spheres. J. Appl. Phys., vol. 22, 1951, pp. 1242-1246.

26. Guttler, A.: Die Miesche Theorie der Beugung Dielektrische Kugeln mit Absorbierendem Kern und Ihre Dedrutung sür Probleme der Interstellaren Materie und des Atmosphärischen Aerosols. Ann. Phys., vol. 11, 1952, pp. 65-98.

27. Wickramsinghe, Nalise C.: Light Scattering Functions for Small Particles with Applications in Astronomy. Adam Hilger, London, 1973.

28. Espenscheid, W. F.; Willis, E.; Matijevic, E.; and Kerker, M.: Aerosol Studies by Light Scattering. J. Coloid Sci., vol. 20, p. 501, 1965.

29. Fenn, R. W.; and Oser, H.: Scattering Properties of Concentric Soot-Water Spheres for Visible and Infrared Light. Appl. Optics, vol. 4, 1965, p. 1504.

30. Pilat, Michael J.: Optical Efficiency Factors for Concentric Spheres. Appl. Opt., vol. 6, 1967, pp. 1555-1558.

31. Cuzzi, Jeffrey N.; and Pollack, James B.: Saturn's Rings: Particle Composition and Size Distribution as Constrained by Microwave Observations. Icarus, vol. 33, 1978, pp. 233-262.

32. Meyer, B.: Sulfur, Energy, and Environment. Elsevier, Amsterdam, 1977.

33. Adams, A. R.; and Spear, W. E.: The Charge Transport in Orthorhombic Sulfur Crystals. J. Phys. Chem. Solids, vol. 25, Oct. 1964, pp. 1113-1118.

34. Lacis, A. A.: Cloud Structure and Heating Rates in the Atmosphere of Venus. J. Atmos. Sci., vol. 32, no. 6, 1975, pp. 1107-1124.

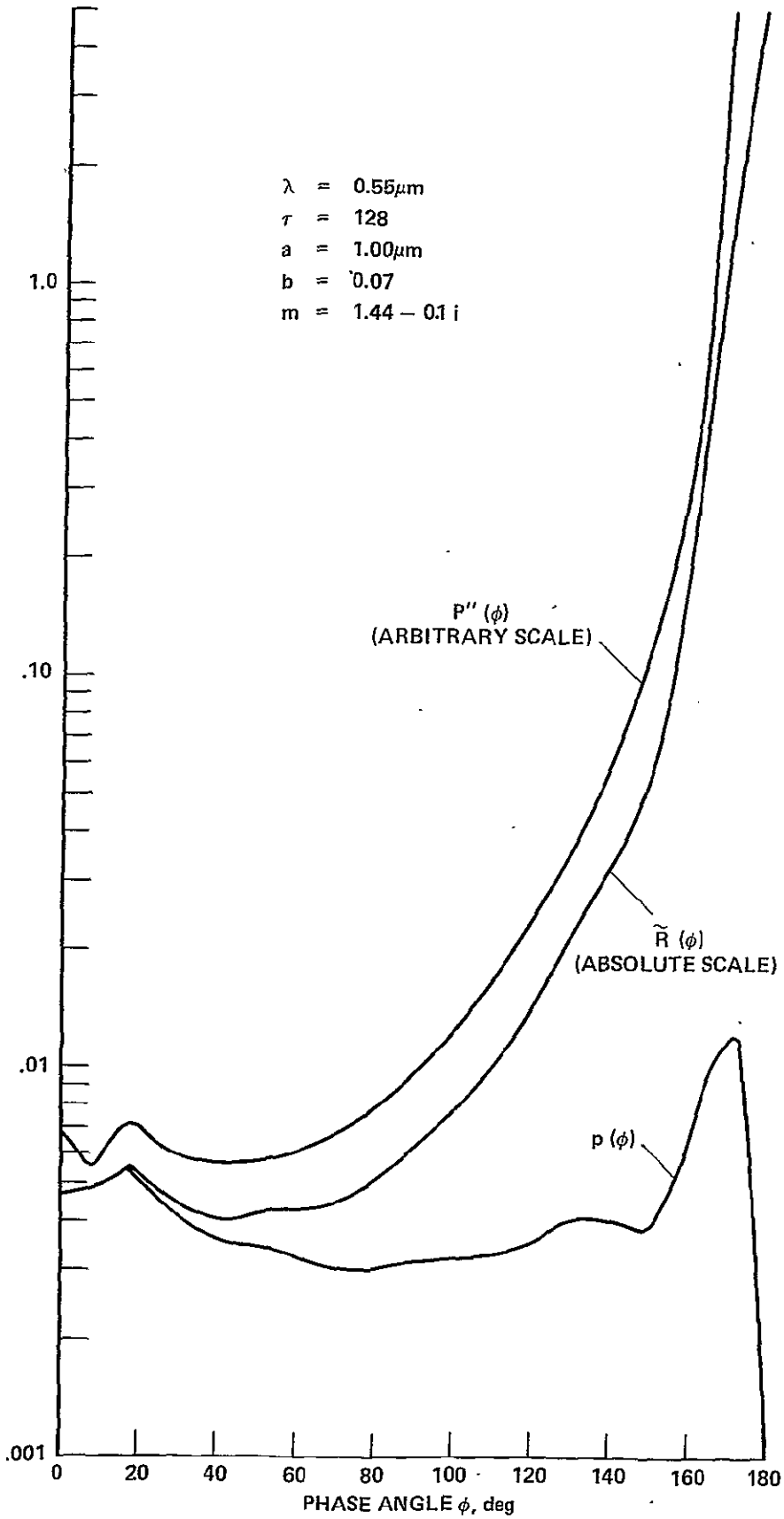

Figure 1.- Reflectivity with strong absorption at a visual wavelength (Hansen and Travis's hypothetical case no. 4, ref. 6); $P''(\phi)$ is the single scattering phase function plotted on an arbitrary scale; $\tilde{R}(\phi)$ and $p(\phi)$ are the reflectivity function and geometric albedo plotted on the same scale.

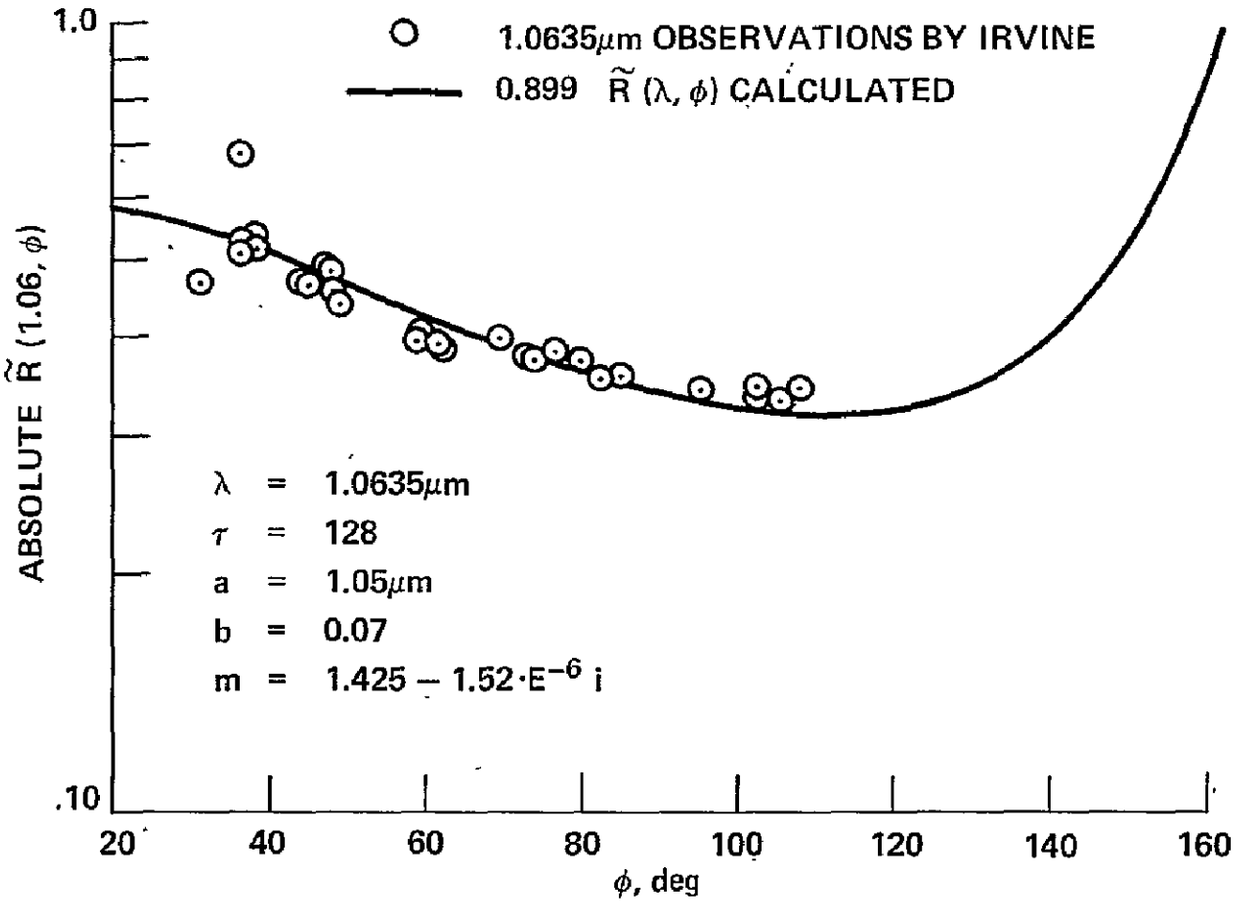

Figure 2.- Observation vs theory at 1.0635 μm. The smooth curve is 0.899 times the calculated reflectivity function; observed data from Irvine et al., (ref. 5).

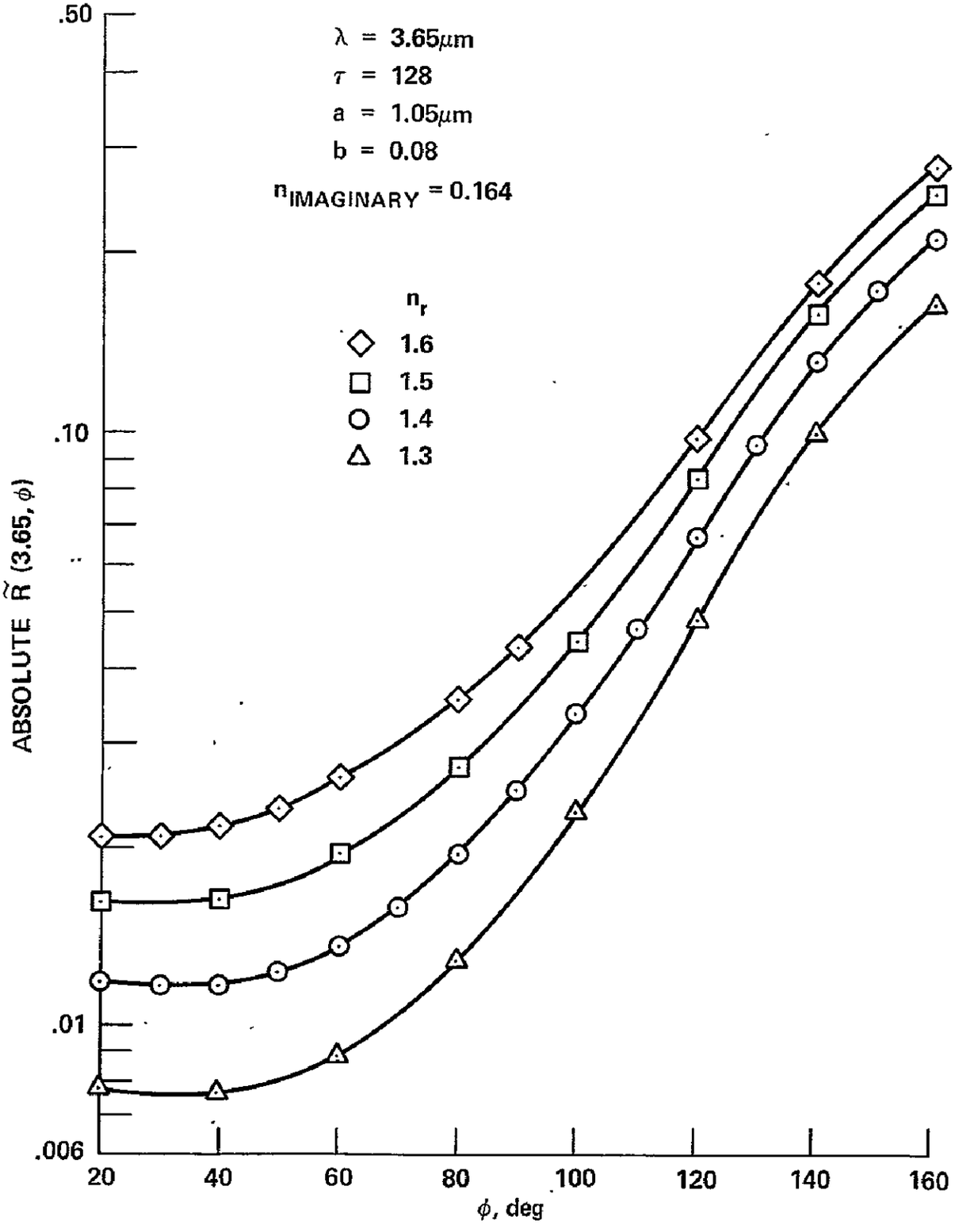

Figure 3.- Variation of the real index in the homogeneous drop model.

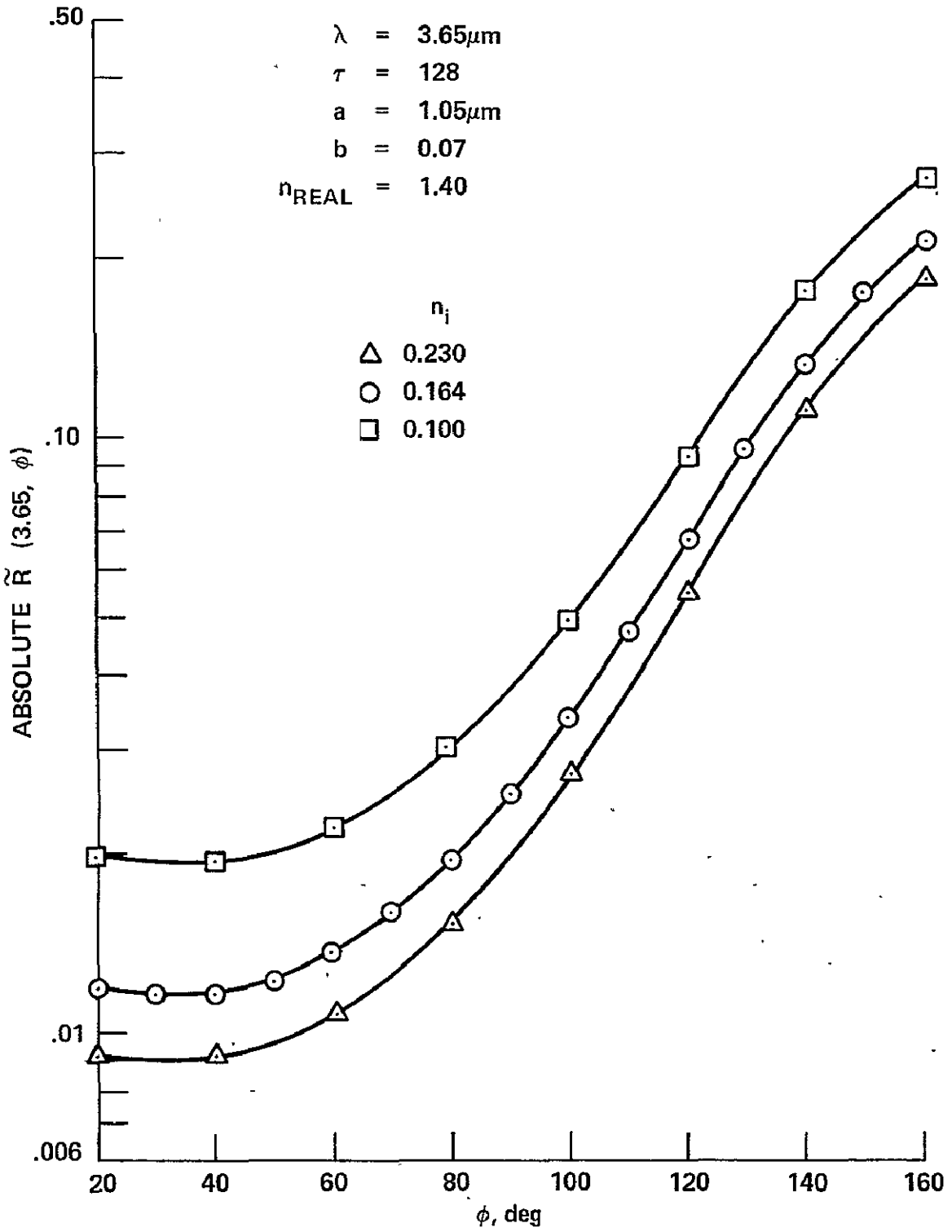

Figure 4.- Variation of the imaginary index in the homogeneous drop model.

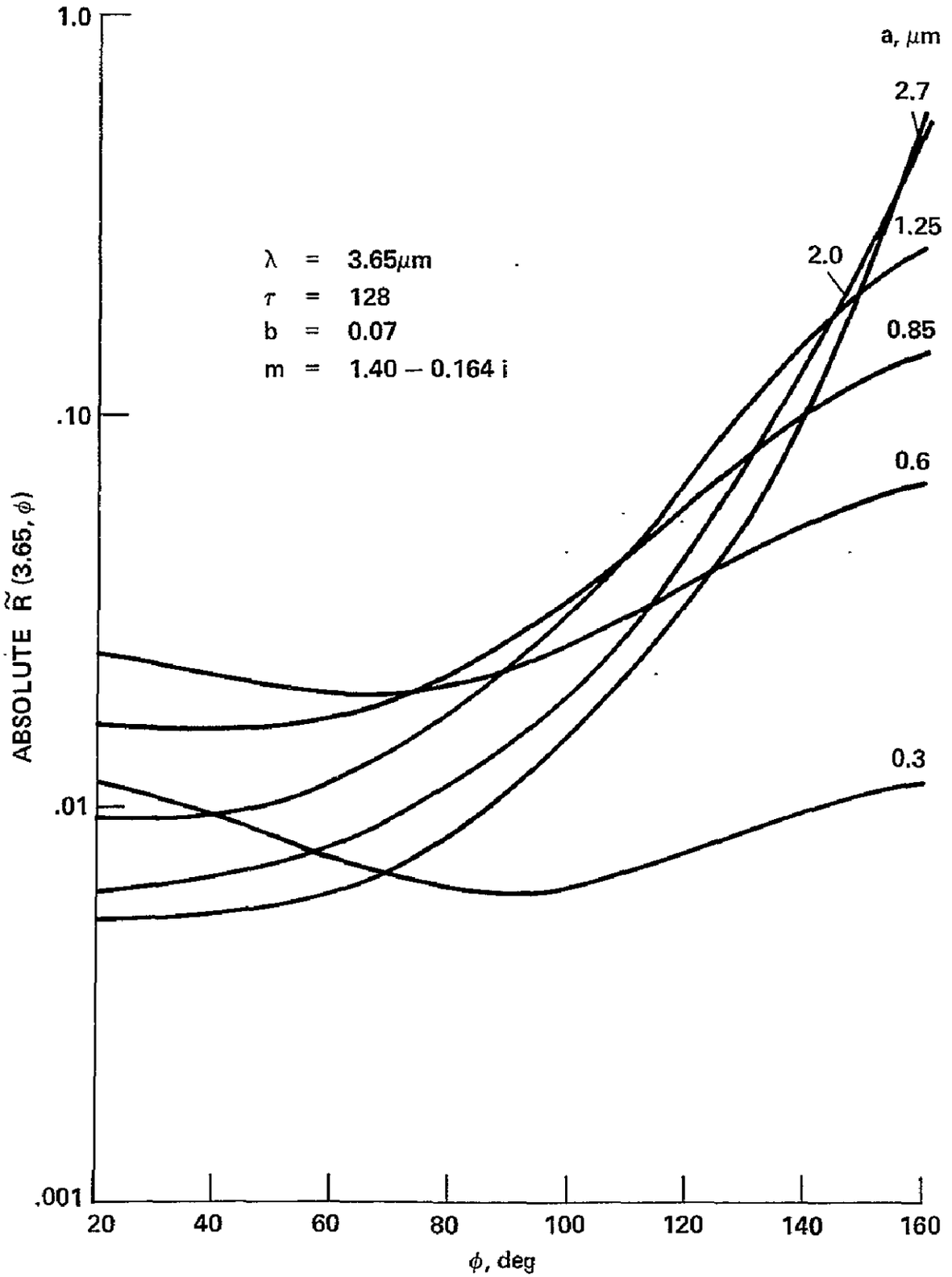

Figure 5.- Variation of the effective radius in the homogeneous drop model.

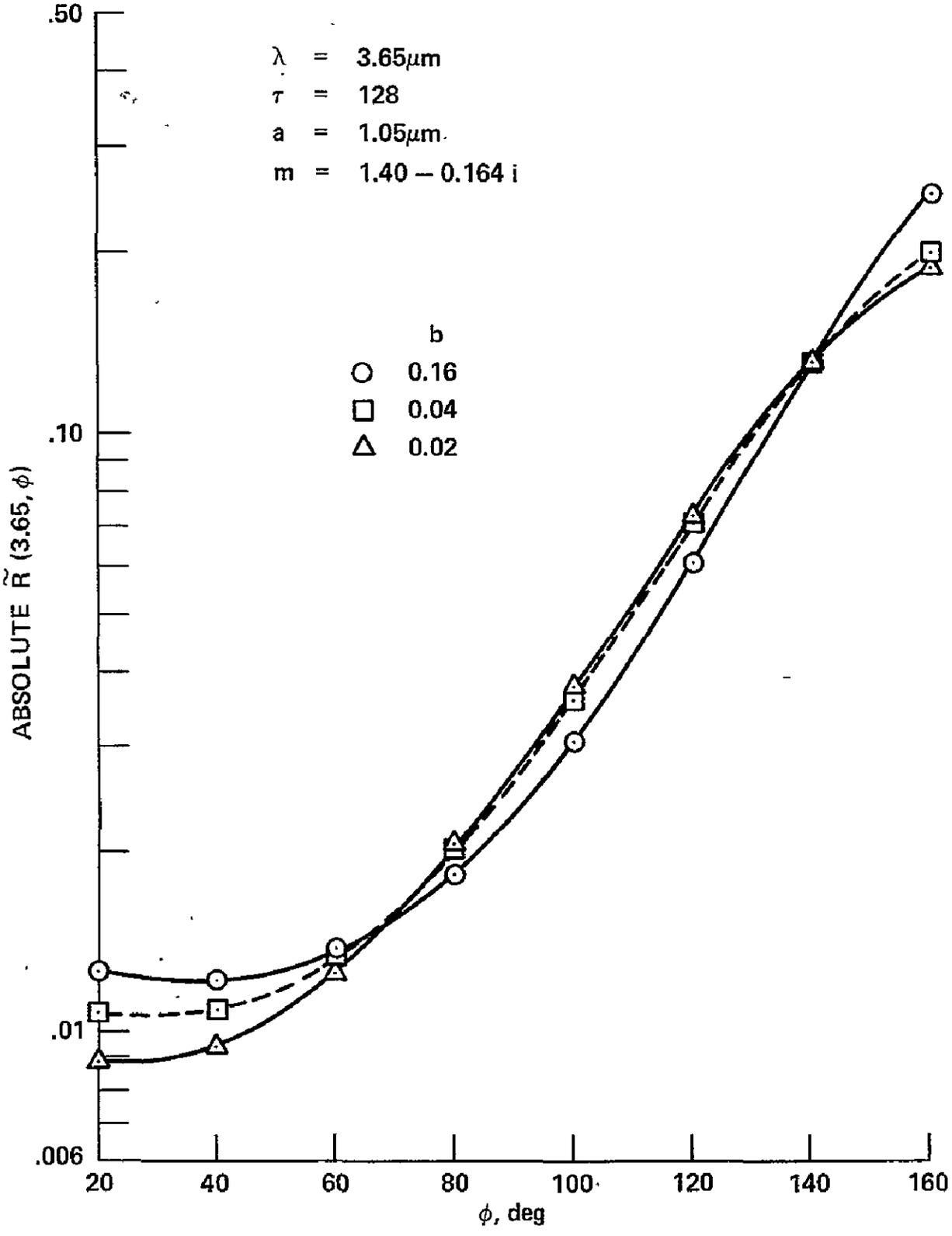

Figure 6.- Variation of the effective variance in the homogeneous drop model.

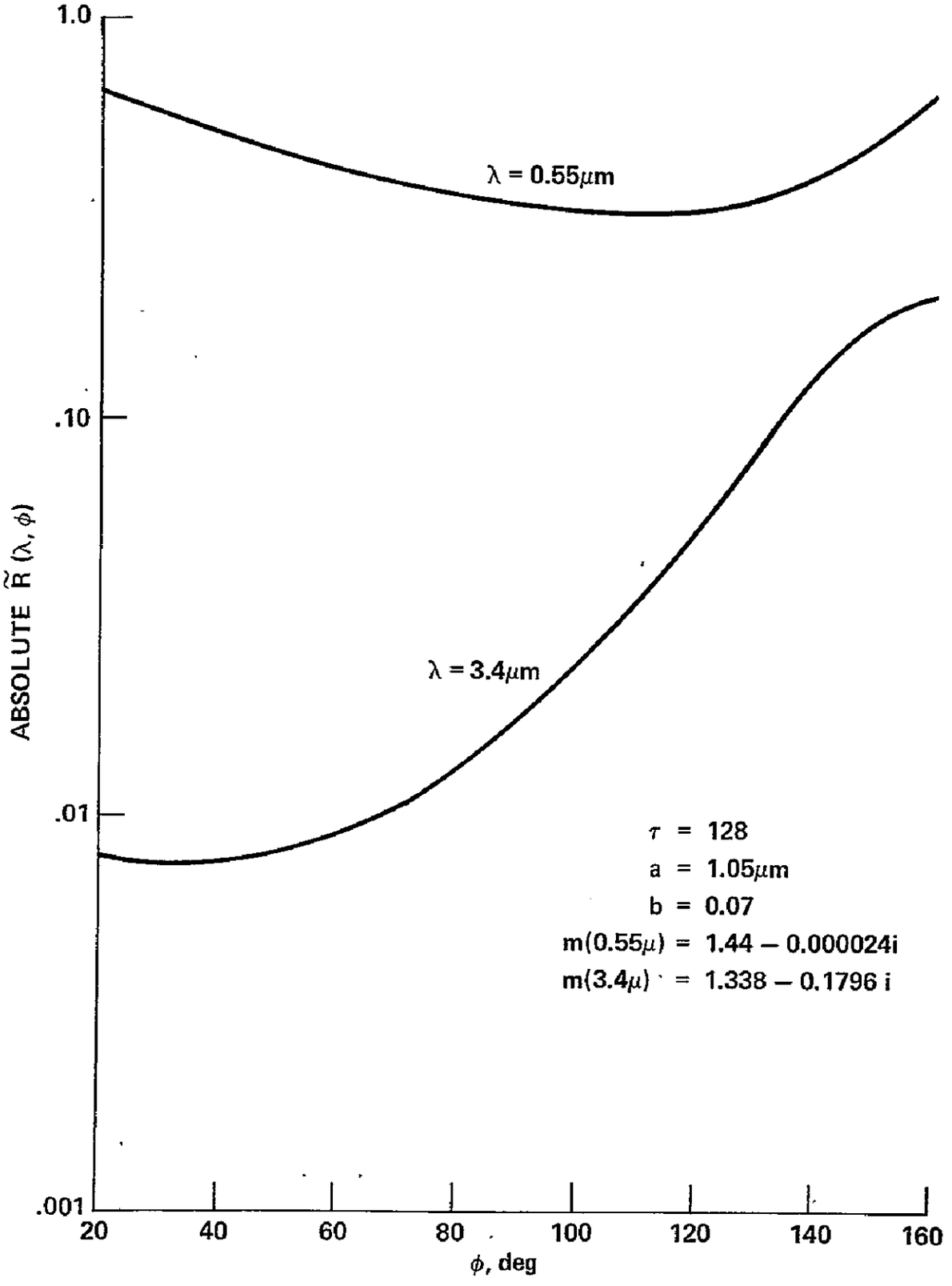

Figure 7.- Variation of the wavelength in the homogeneous drop model.

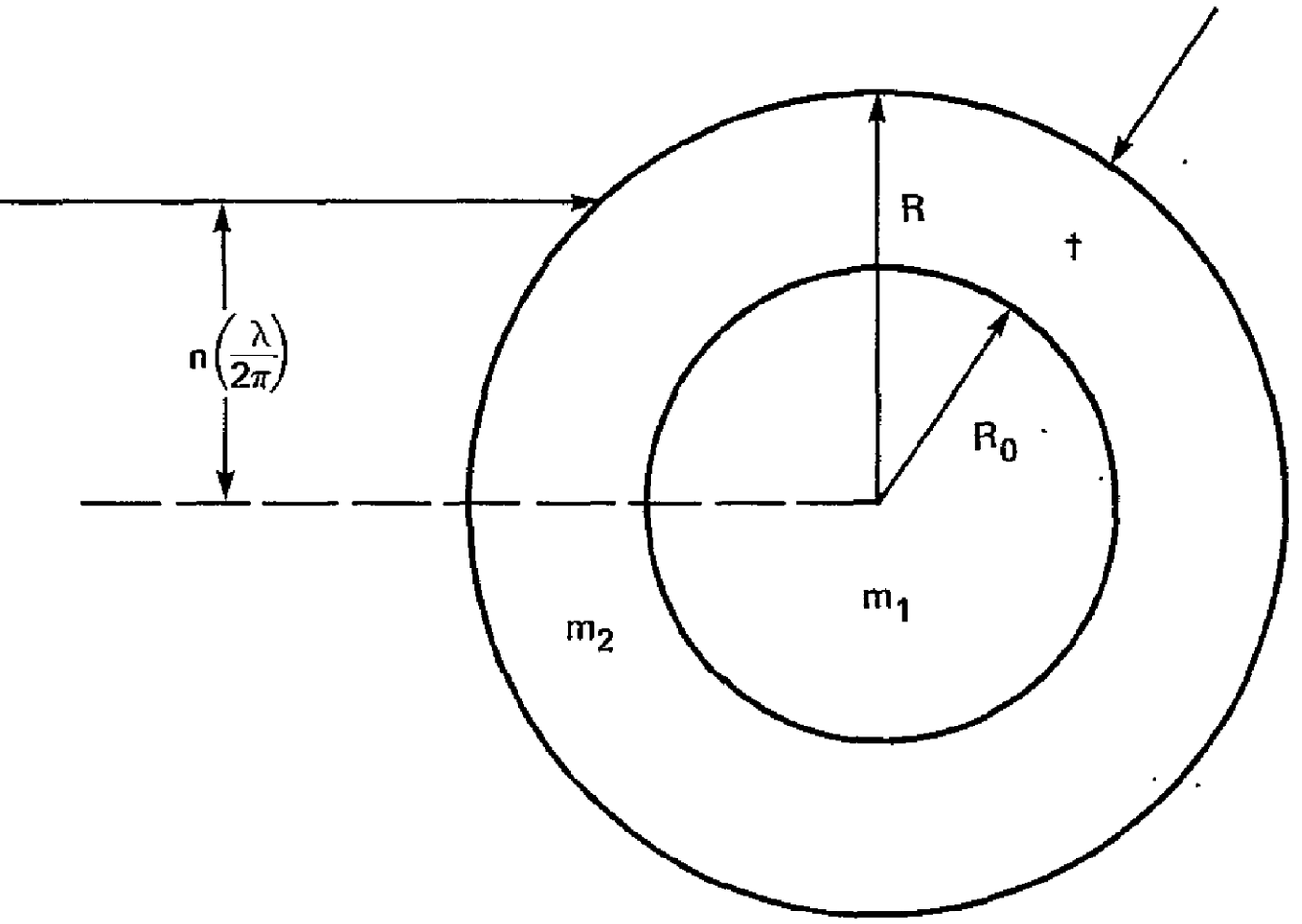

Figure 8.- Inhomogeneous drop.

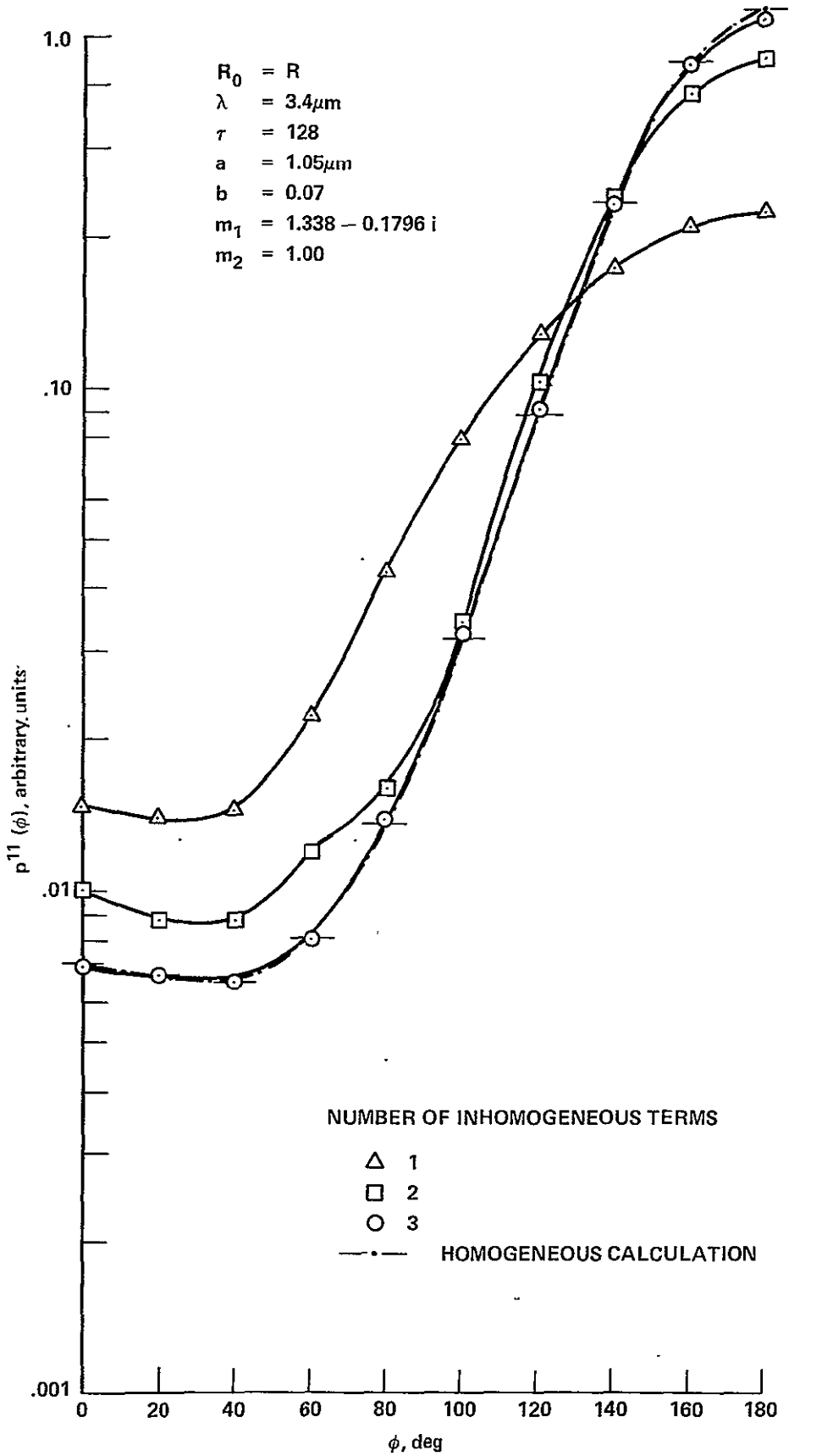

Figure 9.- Single scattering phase functions for equivalence test no. 5 (R_o = R).

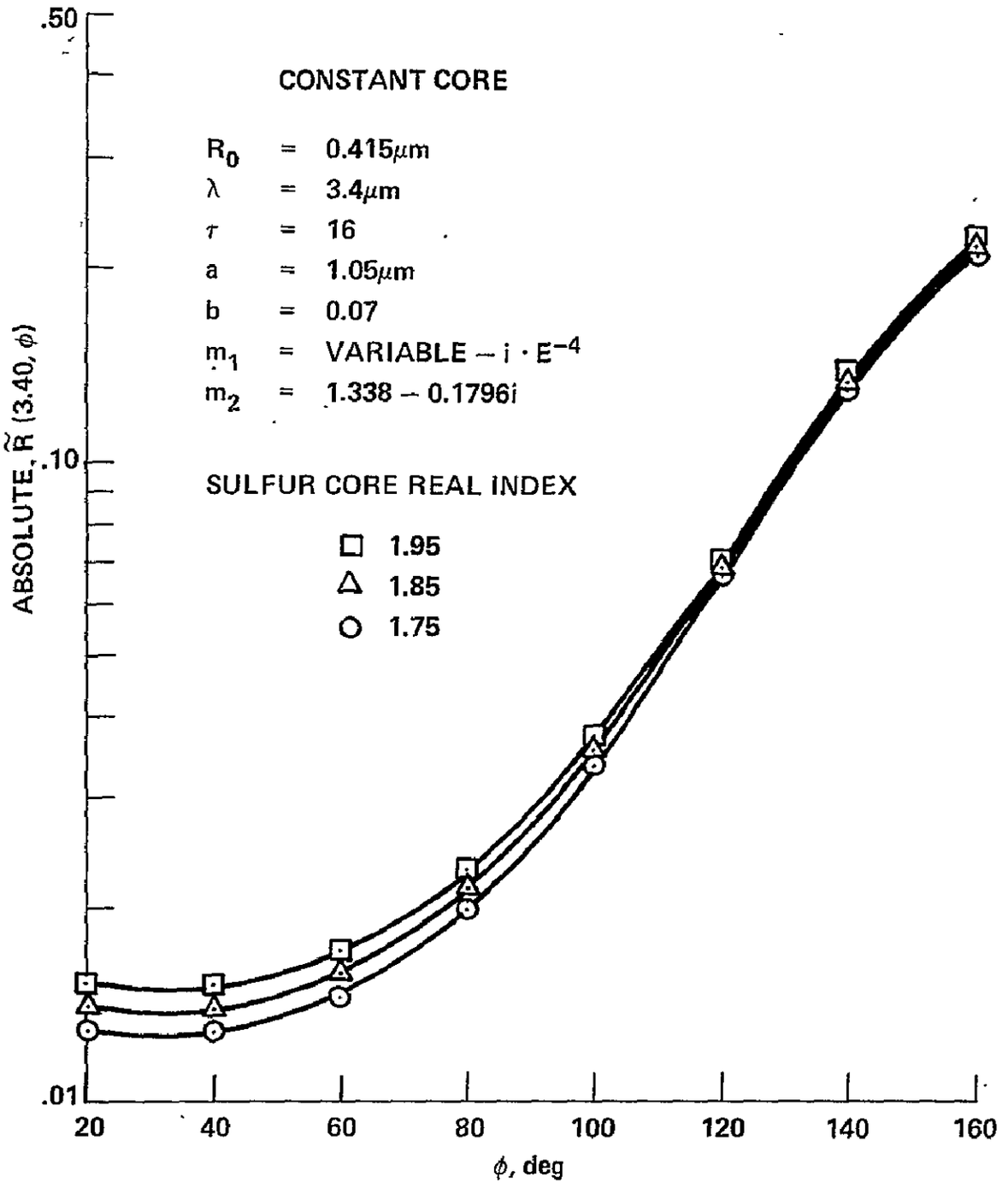

Figure 10.– Variation of real index of core of inhomogeneous drop model: constant core calculation.

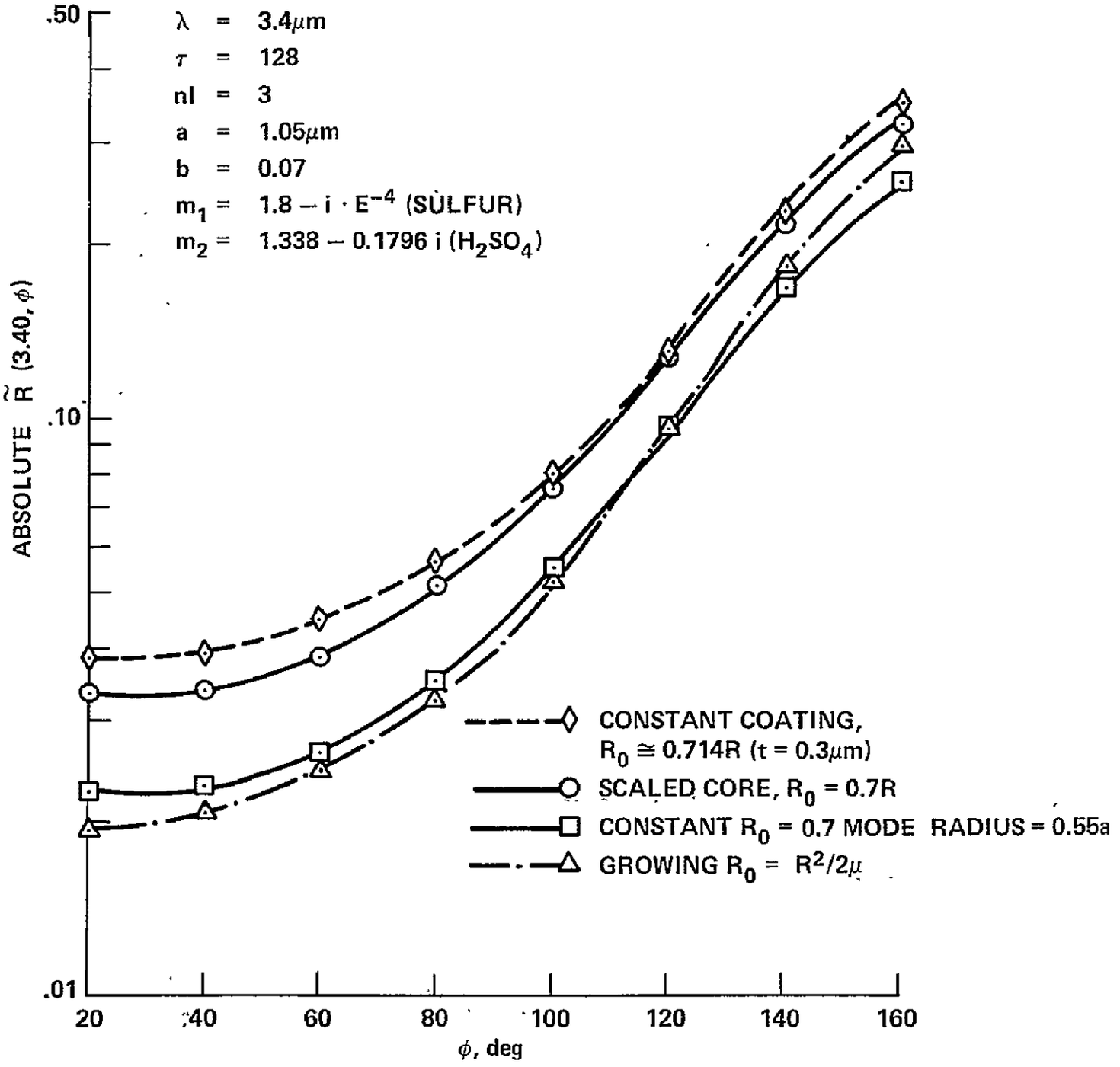

Figure 11.- Comparison of four different ways to vary the core radius of the inhomogeneous drop over the size distribution.

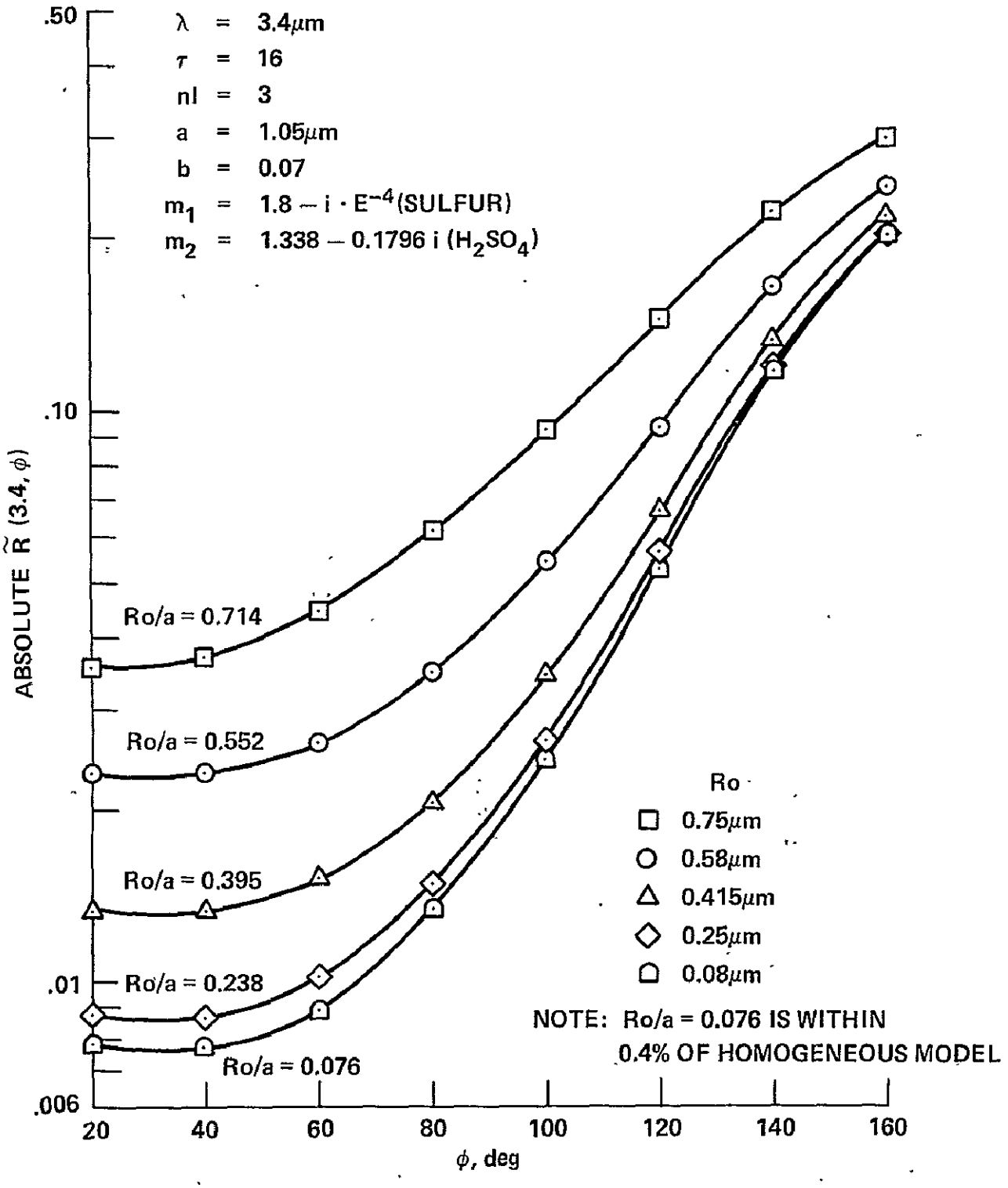

Figure 12.- Variation of thickness of constant coating, inhomogeneous drop model.

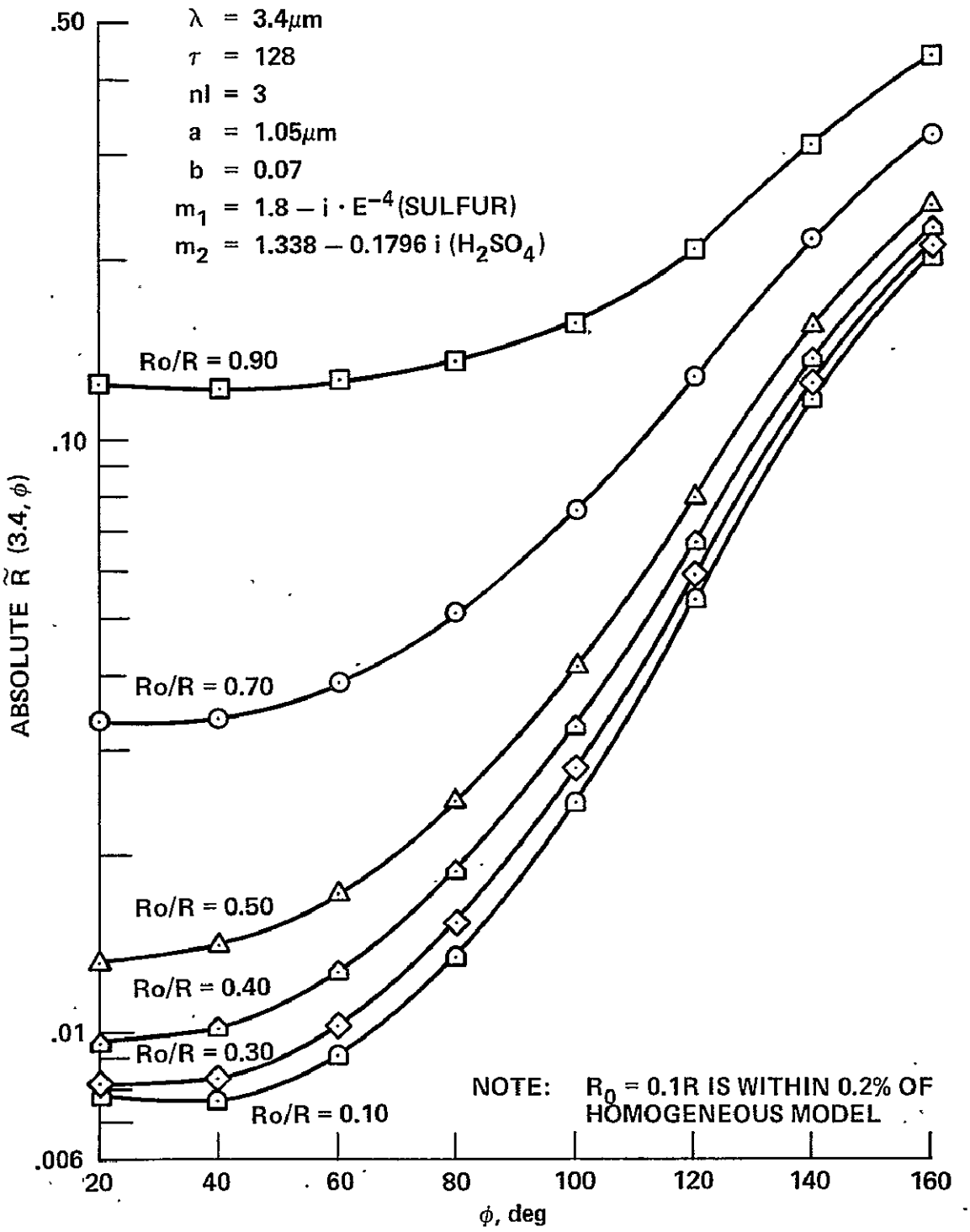

Figure 13.- Variation of size of constant core of inhomogeneous drop model.

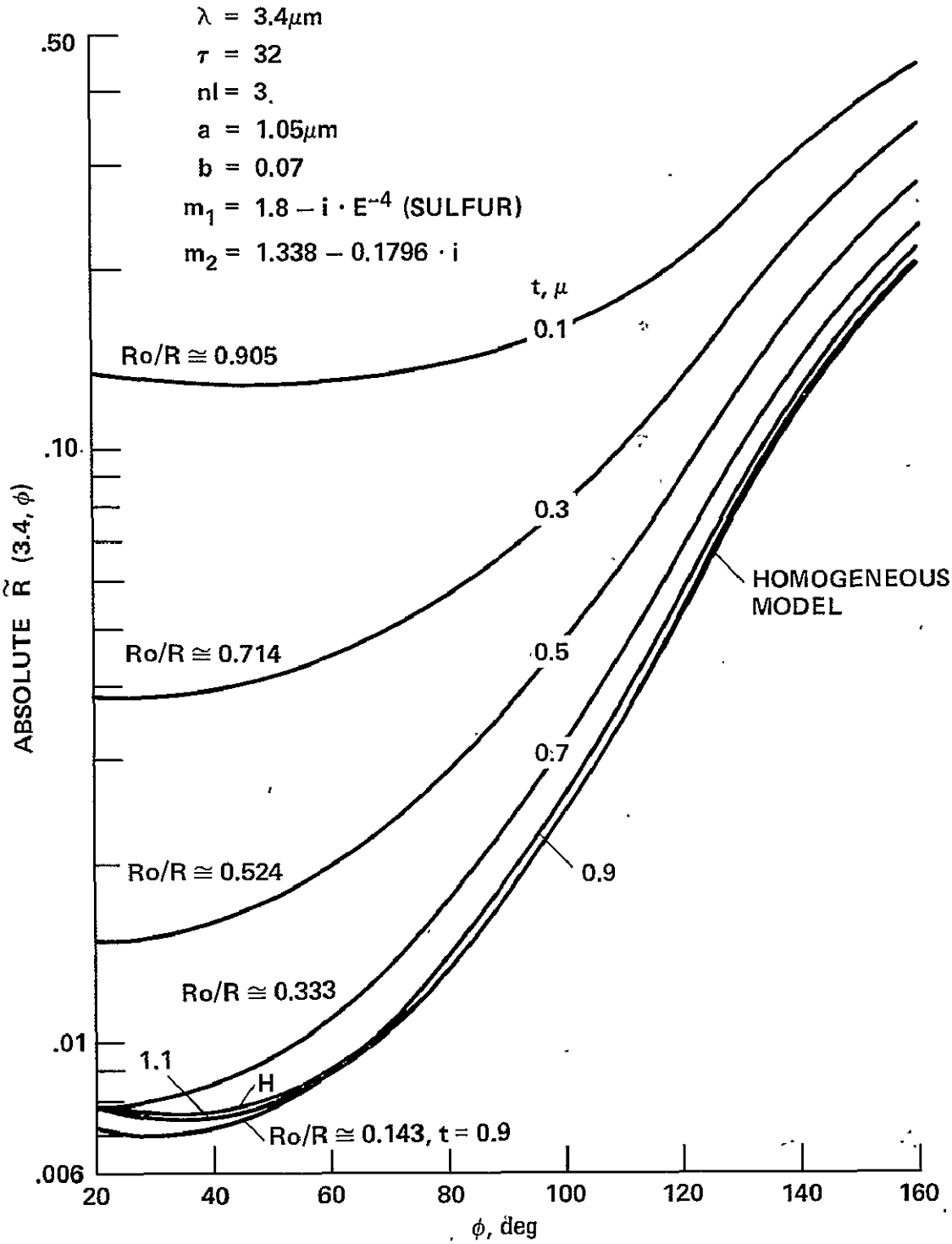

Figure 14.- Variation of size of scaled core of inhomogeneous drop model.

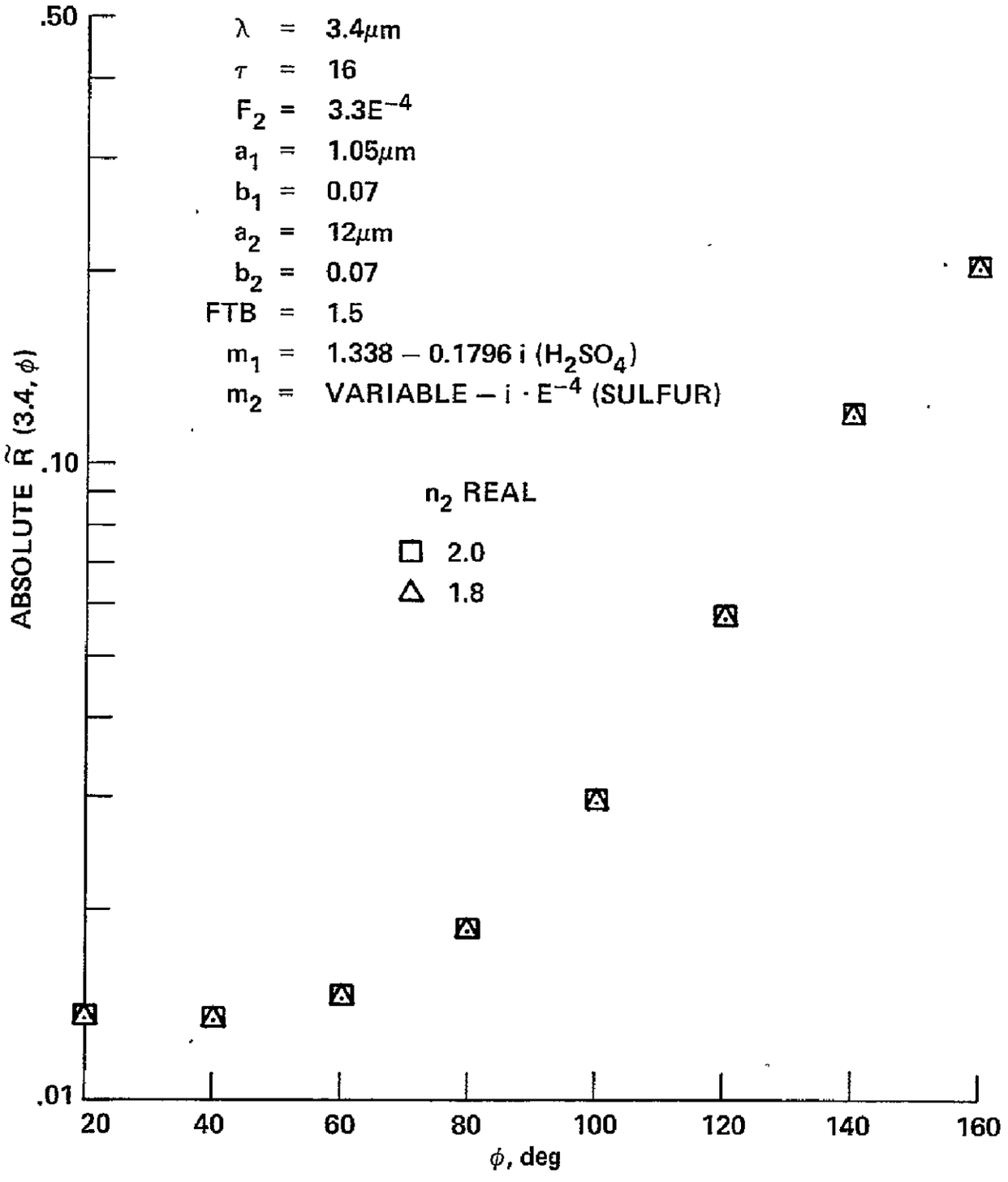

Figure 15.- Variation of real index of sulfur particles of inhomogeneous cloud model.

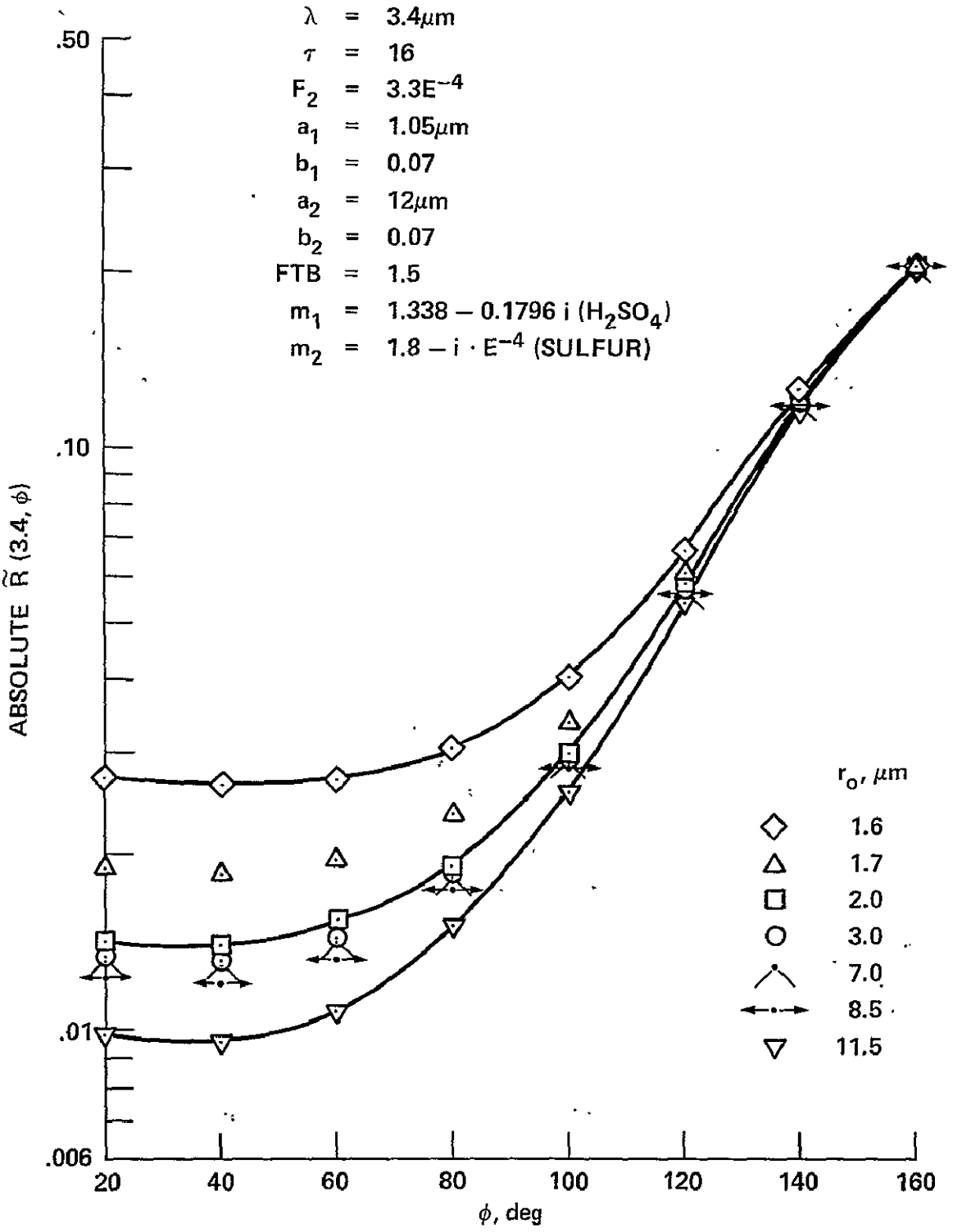

Figure 16.- Variation of r_o of inhomogeneous cloud model.

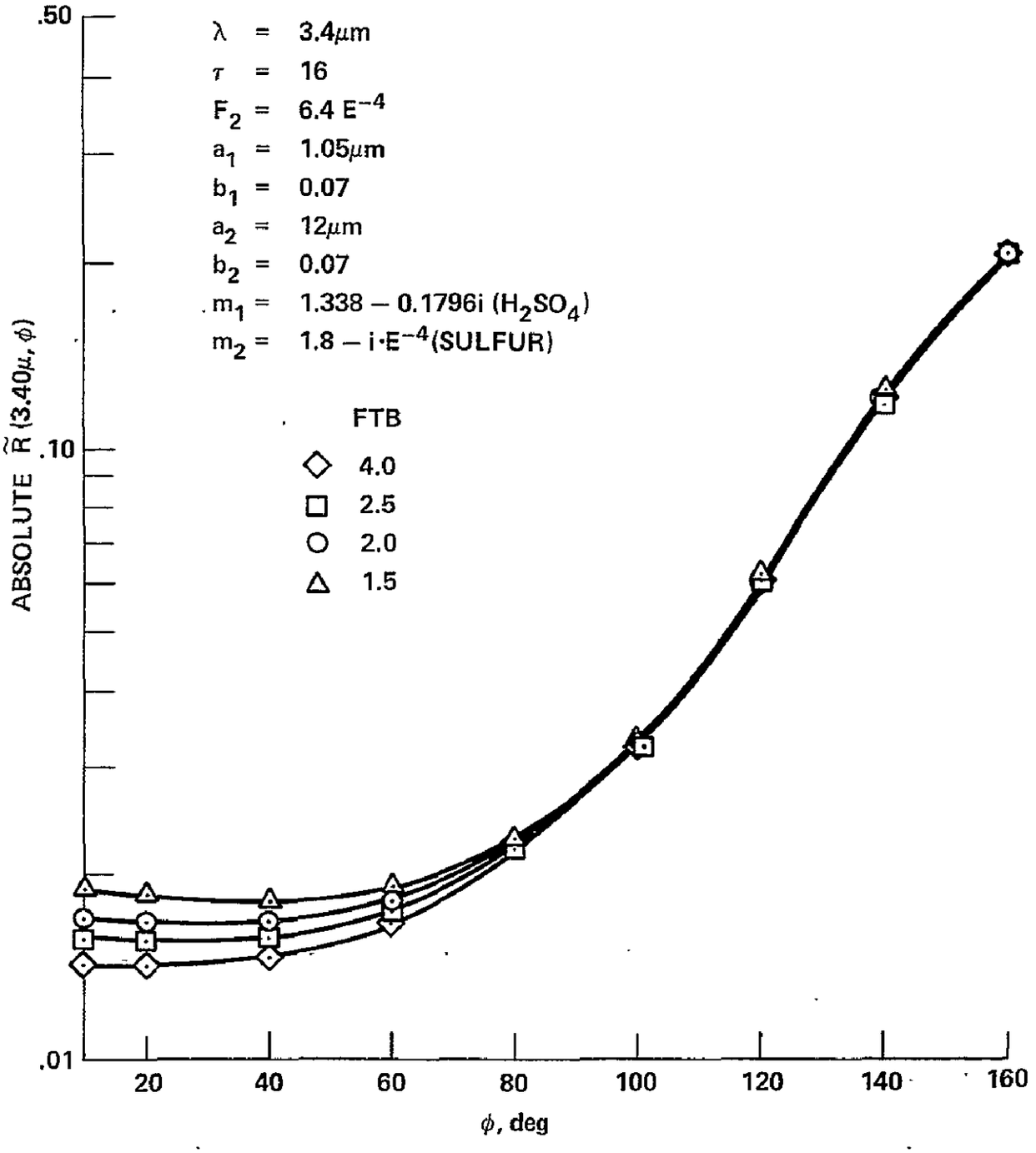

Figure 17.- Variation of FTB of inhomogeneous cloud model.

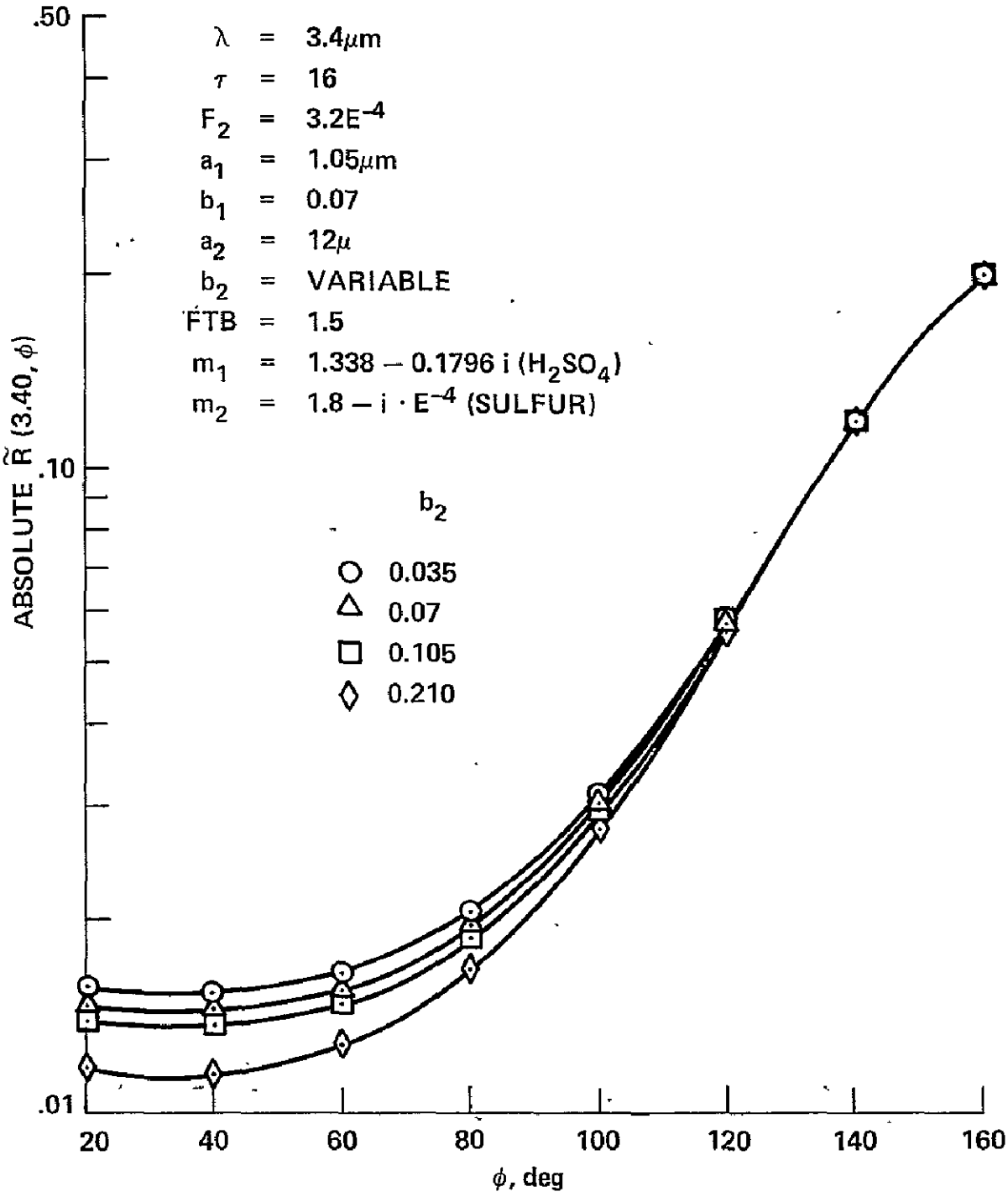

Figure 18.- Variation of b_2 of inhomogeneous cloud model.

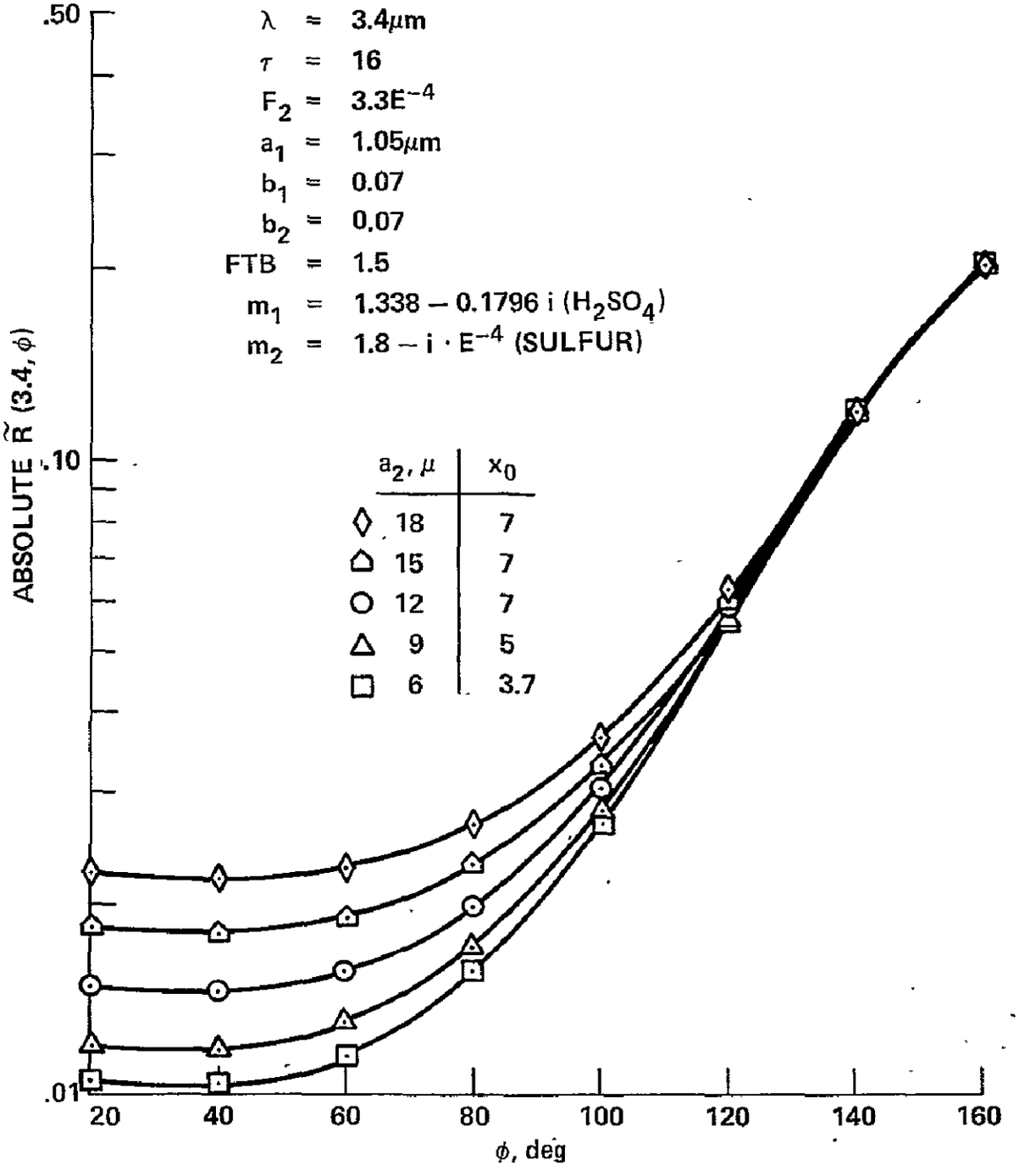

Figure 19.- Variation of effective radius of sulfur particles (a_2) of inhomogeneous cloud model.

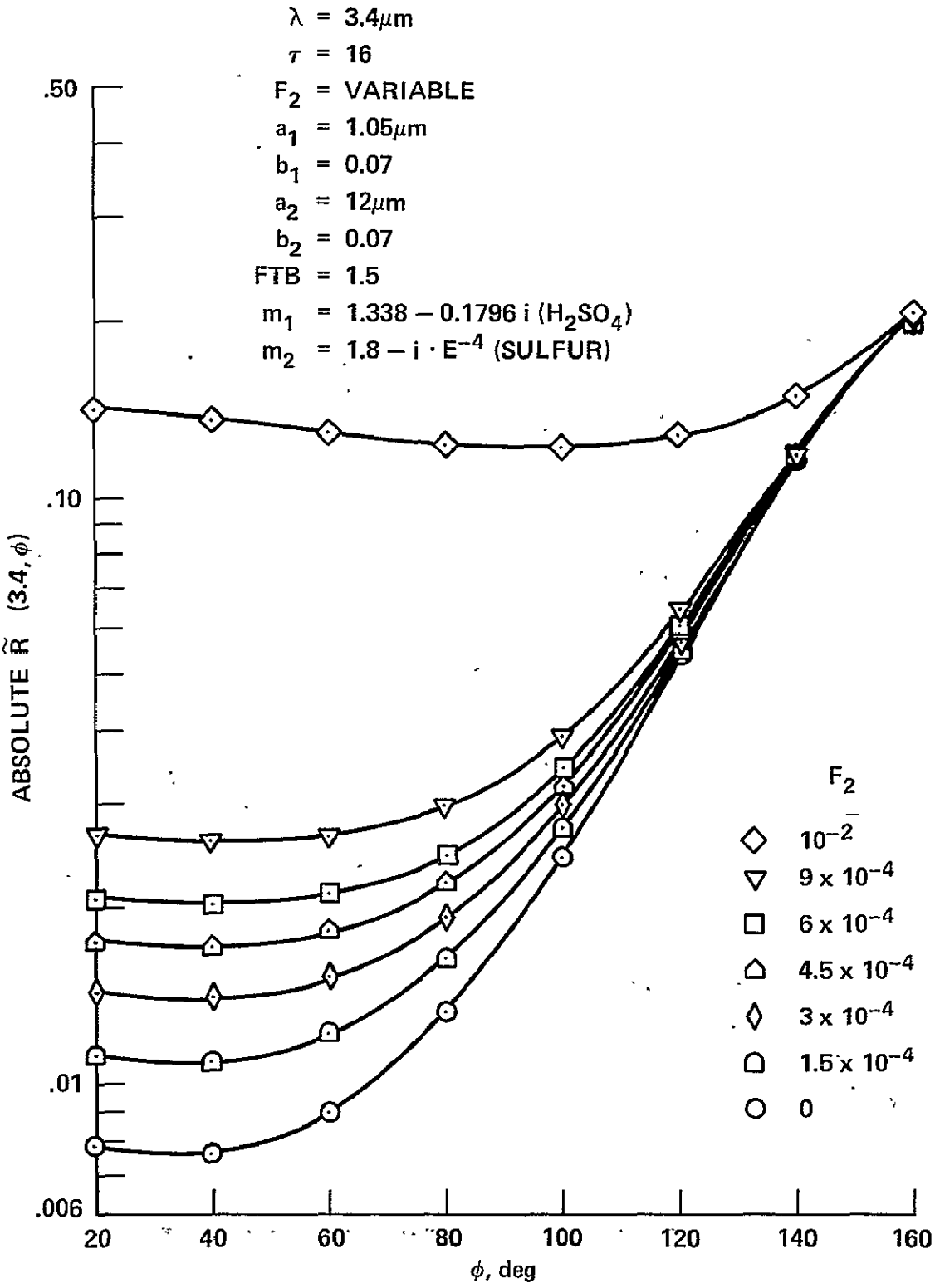

Figure 20.- Variation of the fraction (F_2) of all particles in the sulfur peak of the inhomogeneous cloud model.

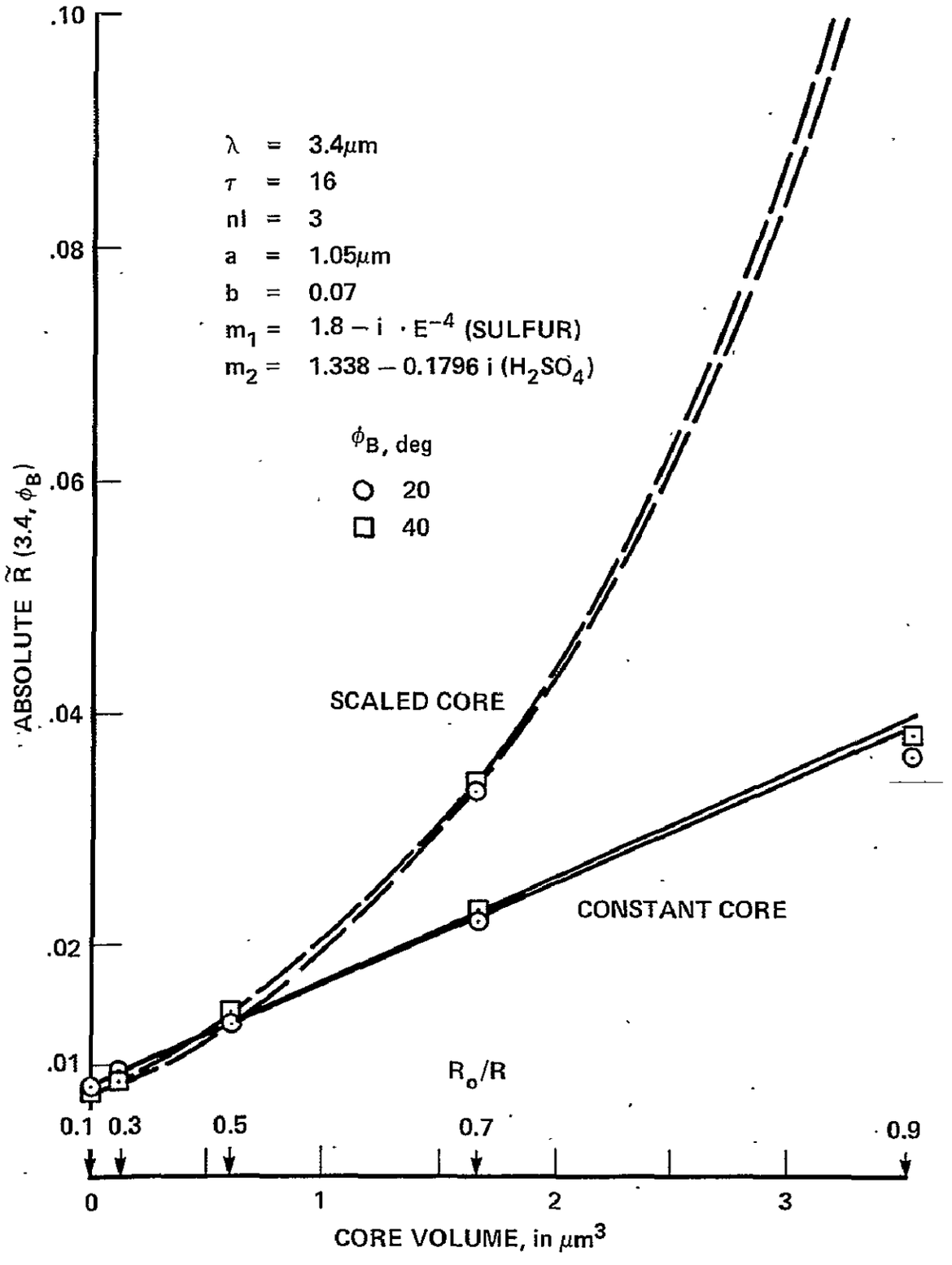

Figure 21.- Dependence of the backscattered reflectivity function $\tilde{R}(3.4,\phi_B)$ upon sulfur core volume in the inhomogeneous drop model; relative core sizes (R_o/R) are indicated by arrows along the abscissa.

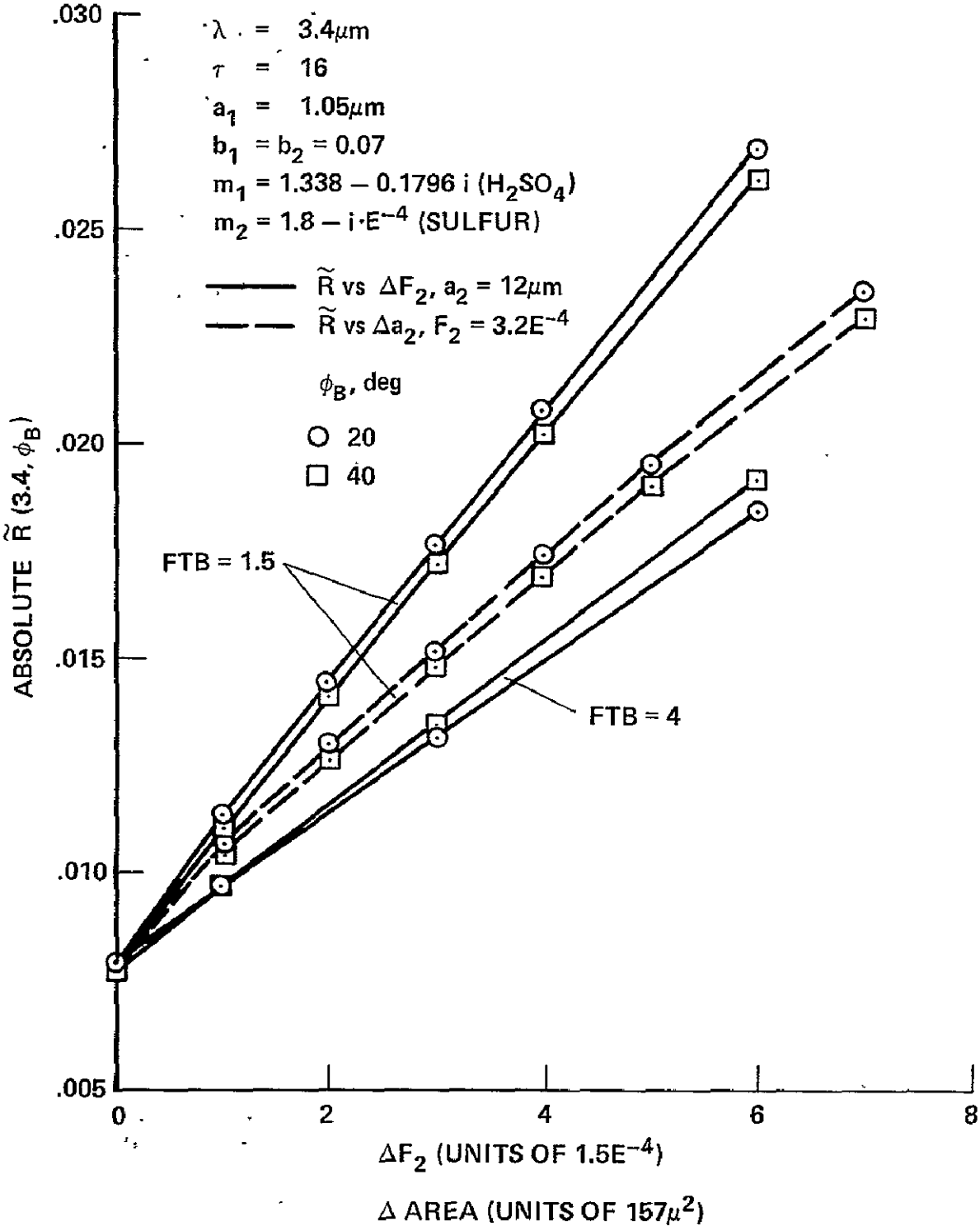

Figure 22.- Dependence of the backscattered reflectivity function $\tilde{R}(3.4,\phi_B)$ upon total particle area in the inhomogeneous cloud model.

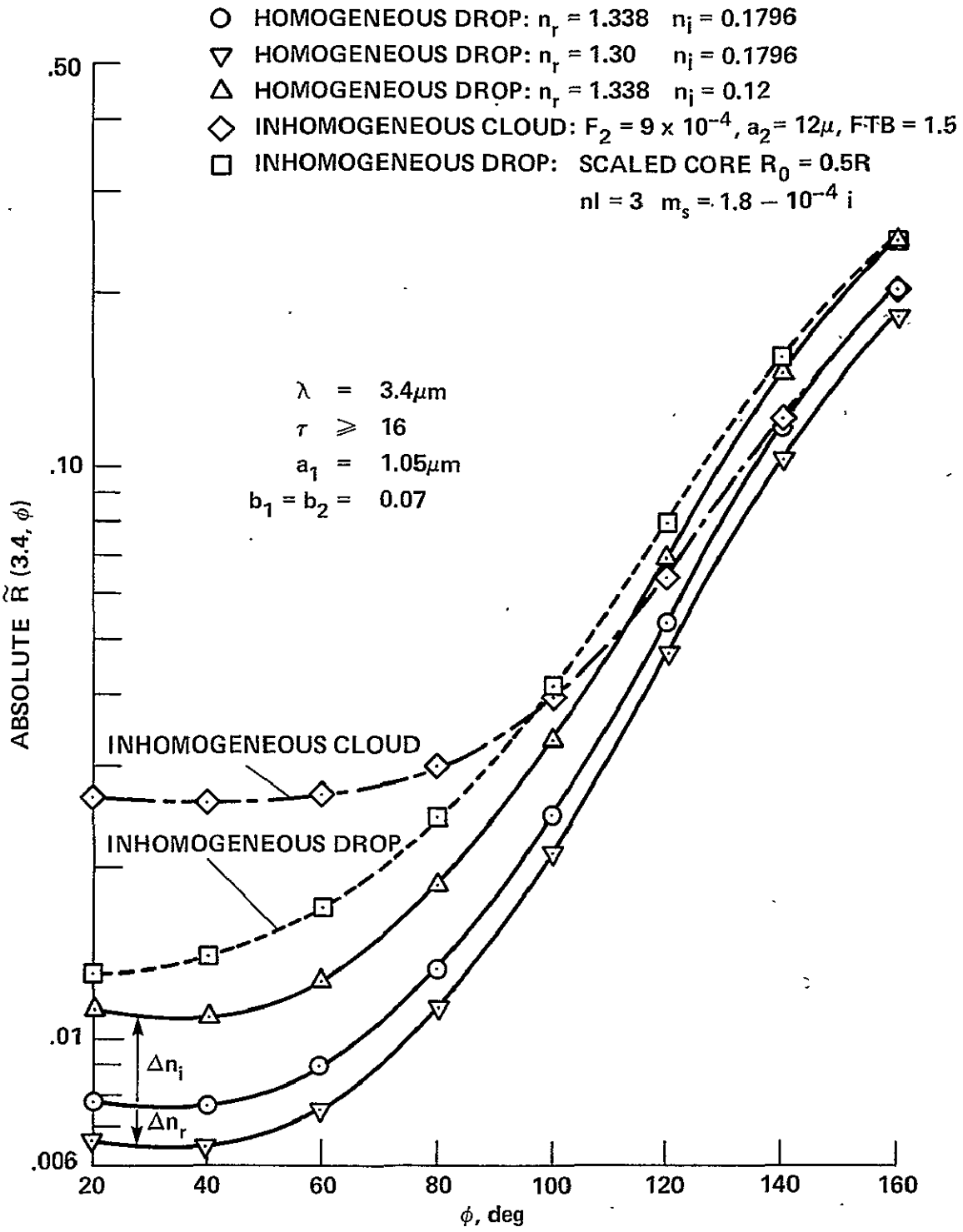

Figure 23.- Comparison of homogeneous and inhomogeneous models.

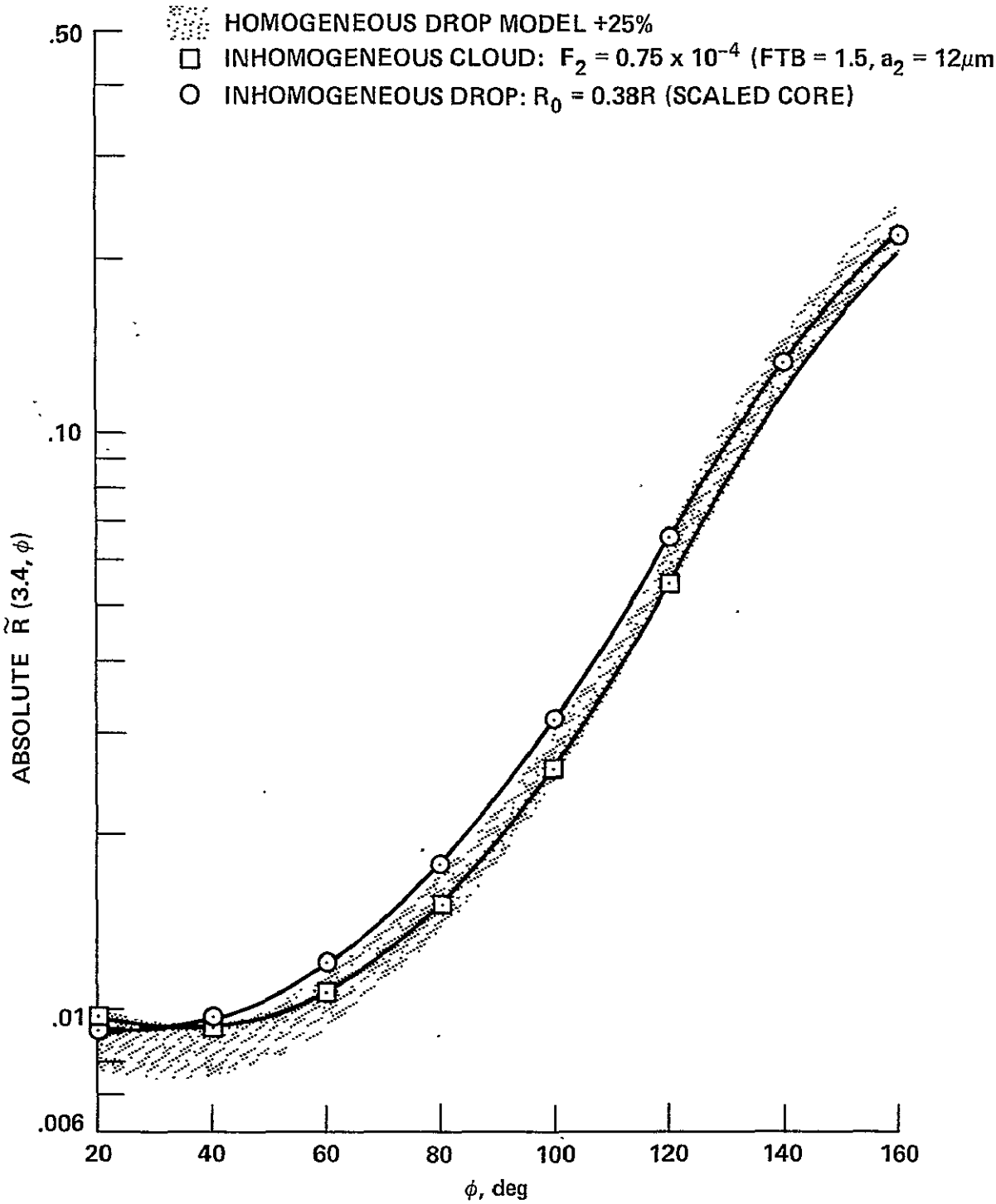

Figure 24.- Sulfur detectability.

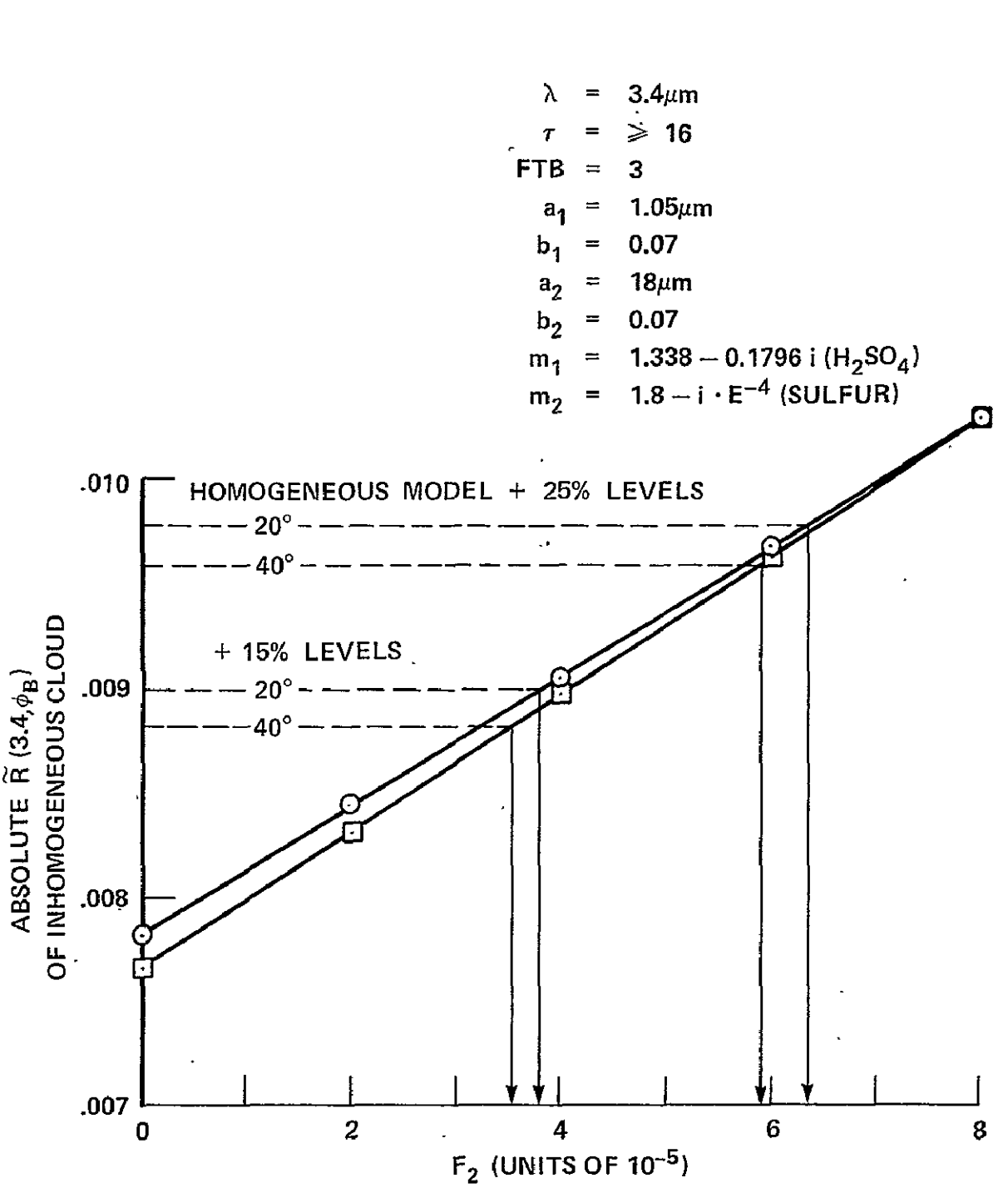

Figure 25.- Detectability limits of inhomogeneous cloud model for a_2 = 18 μm and FTB = 3; minimum distinguishable values of F_2 are indicated by arrows.

1 Report No.	2 Government Accession No	3. Recipient's Catalog No
NASA TM-78558		

4 Title and Subtitle	5. Report Date
INHOMOGENEOUS MODELS OF THE VENUS CLOUDS CONTAINING SULFUR	6. Performing Organization Code

7 Author(s)	8 Performing Organization Report No
Sheldon M. Smith, James B. Pollack, Lawrence P. Giver, Jeffrey N. Cuzzi, and Morris Podolak*	A-7701

9. Performing Organization Name and Address	10 Work Unit No
NASA Ames Research Center Moffett Field, Calif., 94035	195-21-01-01
	11. Contract or Grant No.

12. Sponsoring Agency Name and Address	13 Type of Report and Period Covered
National Aeronautics and Space Administration Washington, D.C. 20546	Technical Memorandum
	14 Sponsoring Agency Code

15. Supplementary Notes

*Tel-Aviv University, Tel-Aviv, Israel

16 Abstract

On the basis of A. T. Young's suggestion that elemental sulfur is responsible for the yellow color of Venus, we compare calculations at 3.4 μm of the reflectivity phase function of two sulfur containing inhomogeneous cloud models with that of the homogeneous model of Hansen and Hovenier. The inhomogeneous drop model has a spherical core of solid sulfur within each sulfuric acid drop, while the inhomogeneous cloud model has a bimodal size distribution with irregular sulfur particles comprising the second size mode near 13 μm. The calculations were made at 3.4 μm because the ability to detect small contributions from non-absorbing species to the sunlight scattered by the Venus clouds is greatly enhanced (~40 times) in the infrared absorption band of sulfuric acid. Assuming reflectivity observations with 25% or less total error, comparison of the model calculations leads to a minimum detectable mass of sulfur equal to 7% of the mass of sulfuric acid for the inhomogeneous drop model. For the inhomogeneous cloud model the comparison leads to a minimum detectable mass of sulfur between 17% and 38% of the mass of the acid drops, depending upon the actual size of the large particles. That amount of sulfur is equivalent to detecting about one large sulfur particle per 10^4 sulfuric acid drops. We conclude that moderately accurate 3.4 μm reflectivity observations are capable of detecting quite small amounts of elemental sulfur at the top of the Venus clouds.

17 Key Words (Suggested by Author(s))	18 Distribution Statement
Space science Astronomy Venus Inhomogeneous models	Unlimited STAR Category - 89

19. Security Classif. (of this report)	20 Security Classif. (of this page)	21 No. of Pages	22. Price*
Unclassified	Unclassified	56	$4.50

*For sale by the National Technical Information Service, Springfield, Virginia 22161.